AGU PUBLICATIONS

Earth's Future

RESEARCH ARTICLE
10.1002/2015EF000304

Key Points:
- WRF adds significant value beyond CCSM4
- Bias correction of GCMs does not always reduce model bias
- Extreme precipitation is projected to increase

Supporting Information:
- Supporting Information S1

Corresponding Author:
J. Wang, jialiwang@anl.gov

Citation:
Wang, J., and V. R. Kotamarthi (2015), High-resolution dynamically downscaled projections of precipitation in the mid and late 21st century over North America, *Earth's Future*, *3*, 268–288, doi:10.1002/2015EF000304.

Received 18 MAR 2015
Accepted 7 JUN 2015
Accepted article online 14 JUL 2015
Published online 29 JUL 2015

High-resolution dynamically downscaled projections of precipitation in the mid and late 21st century over North America

Jiali Wang[1] and Veerabhadra R. Kotamarthi[1]

[1] Environmental Science Division, Argonne National Laboratory, Lemont, Illinois, USA

Abstract This study performs high-spatial-resolution (12 km) Weather Research and Forecasting (WRF) simulations over a very large domain (7200 km × 6180 km, covering much of North America) to explore changes in mean and extreme precipitation in the mid and late 21st century under Representative Concentration Pathways 4.5 (RCP 4.5) and 8.5 (RCP 8.5). We evaluate WRF model performance for a historical simulation and future projections, applying the Community Climate System Model version 4 (CCSM4) as initial and boundary conditions with and without a bias correction. WRF simulations using boundary and initial conditions from both versions of CCSM4 show smaller biases versus evaluation data sets than does CCSM4 over western North America. WRF simulations also improve spatial details of precipitation over much of North America. However, driving the WRF with the bias-corrected CCSM4 does not always reduce the bias. WRF-projected changes in precipitation include decreasing intensity over the southwestern United States, increasing intensity over the eastern United Sates and most of Canada, and an increase in the number of days with heavy precipitation over much of North America. Projected precipitation changes are more evident in the late 21st century than the mid 21st century, and they are more evident under RCP 8.5 than under RCP 4.5 in the late 21st century. Uncertainties in the projected changes in precipitation due to different warming scenarios are non-negligible. Differences in summer precipitation changes between WRF and CCSM4 are significant over most of the United States.

1. Introduction

The potential impacts of anticipated climate changes have received a great deal of attention from researchers in a variety of fields [e.g., *Diffenbaugh et al*., 2013; *Blanc et al*., 2014; *Bowles et al*., 2014; *Kyle et al*., 2014; *Kumar et al*., 2014]. The enhancement in precipitable water due to an atmospheric temperature increase can change spatial and temporal variations of precipitation characteristics on regional and global scales [*Meehl et al*., 2000; *Giorgi et al*., 2011; *Janssen et al*., 2014; *Wuebbles et al*., 2014]. The greatest threat to humans (and other components of terrestrial ecosystems) will be manifested locally via changes in regional extreme weather and climate events. The primary tool to study anticipated climate changes at the regional/local scale is the emerging technique called "downscaling." The two downscaling approaches are (1) dynamic methods, involving the explicit solving of the process-based physical dynamics of the system [e.g., *Giorgi and Mearns*, 1991; *Xu*, 1999], and (2) statistical methods that use identified system relationships derived from observational data [e.g., *Hewitson and Crane*, 1992; *Hayhoe et al*. 2004; *Stoner et al*. 2012]. Although the statistical method is much less computationally demanding, it is limited in the number of variables that can be downscaled, and its performance relies significantly on long-term observational data series of good quality. The dynamic method enables simulation of many more variables and is not limited to locations with observational data. It also allows simulations of greater topographic complexity and finer-scale atmospheric dynamics, improving spatial resolution by factors of 2–10 versus the driving global model. This capability could, in principle, allow modelers to represent information required for studies of regional climate change and its impacts [*Zhao et al*., 2011; *Sobolowski and Pavelsky*, 2012; *Oh et al*., 2014; *Gao et al*., 2012; 2014; *Trail et al*., 2013; *Lauer et al*., 2013; *Ezer and Atkinson*, 2014; *d'Orgeville et al*., 2014; *Lau and Nath*, 2014; *Gensini and Mote*, 2015].

Many studies use the dynamical downscaling approach to project future climate change, often with model products of the third phase of the Coupled Model Intercomparison Project (CMIP3). For example, three major international programs use CMIP3 results as boundary conditions to project the future climate with

regional-scale models. Two of the programs are for Europe—the Prediction of Regional Scenarios and Uncertainties for Defining European Climate Change Risks and Effects (PRUDENCE) [*Christensen et al*., 2007] and ENSEMBLES [*van der Linden and Mitchell*, 2009; *Christensen et al*., 2010]. The program for North America is the North American Regional Climate Change Assessment Program (NARCCAP) [*Mearns et al*., 2009, 2013; *Sobolowski and Pavelsky*, 2012; *Loikith et al*., 2015]. With participation from over 20 modeling groups and more than 40 global models, the fifth phase of CMIP (CMIP5) represents the latest, most ambitious coordinated international climate model intercomparison exercise to date [*Taylor et al*., 2012]. CMIP5 runs are designed to simulate projected changes in climate due to changes in greenhouse gases and aerosols by following the scenarios explored by the Representative Concentration Pathways (RCP). In addition to physical improvements made in many models [*Taylor et al*., 2012], one advantage of CMIP5 versus CMIP3 is significantly increased horizontal resolution of the atmospheric components of coupled models. For more comparisons between model products and performance of CMIP3 and CMIP5, see *Taylor et al*. [2012] and *Sillmann et al*. [2013a, 2013b].

The Coordinated Regional Climate Downscaling Experiment (CORDEX) has built a climate projection framework based on CMIP5 model simulations [*Giorgi et al*., 2009], and several institutes and universities have been generating regional climate model (RCM) simulations over the CORDEX North America domain, driven by various global climate models (GCMs; https://na-cordex.org/simulations). The standard spatial resolution recommended by CORDEX is 50 km, but groups are encouraged to explore the benefits of increased model resolution. The model outputs generated by our study will contribute to CORDEX North America.

High-resolution (<20 km) RCMs resolve spatial and temporal dependences much better than do GCMs. For example, *Wang et al*. [2015] found that an RCM at 12 km spatial resolution captures significantly more details of the spatial and temporal variations of precipitation (especially over mountainous regions) than does the 2.5-degree National Centers for Environmental Prediction-U.S. Department of Energy Reanalysis II (NCEP-R2), even when the RCM is aggregated to the grid resolution of NCEP-R2. *Di Luca et al*. [2012] showed that RCMs add high value for warm-season precipitation over short temporal scales, especially over regions of complex topography. Since RCMs require far more computational resources than do GCMs, RCM simulations are generally performed over limited time slices. The NARCCAP simulated two 30 year periods, 1970–2000 and 2040–2070 [*Mearns et al*., 2012], by using six RCMs driven by different GCMs over North America. These products provide the community with a resource for investigating future climate change and a model data set that can be used for estimating uncertainties in a multi-model ensemble on regional scales. However, these RCM simulations were performed at a spatial resolution of 50 km, and they only considered one future scenario (the "A2" scenario applied in CMIP3) because of computational and fiscal constraints. *Pryor et al*. [2012] noted that an increase in RCM resolution from 50 to 6 km captures extreme wind speeds more realistically. *Vautard et al*. [2013] found that heat extremes in Europe were generally better simulated in RCMs with resolution of 12 km versus 50 km. *Tripathi and Dominguez* [2013] found that 10 km simulation captures individual extreme summer precipitation events better than 50 km simulation. On the other hand, future projections of climate and extremes depend largely on projected future greenhouse gas concentration scenarios [e.g., *d'Orgeville et al*., 2014; *Oh et al*., 2014; *Hawkins and Sutton*, 2009; *Hawkins and Sutton*, 2011].

Future projections made by RCMs are distinct from historical simulations in one critical aspect. Although the historical simulations can use observationally derived boundary conditions, the projections have to rely on GCMs to provide these boundary and initial conditions. This adds a significant unknown to the projections generated by RCMs. The model-observational differences in GCMs are generally shown to be reasonable at global scales, but the low skill of GCMs in simulating regional-scale phenomena has been documented extensively [e.g., *Liang et al*., 2008; *Bukovsky and Karoly*, 2011; *Gao et al*., 2012; *Oh et al*., 2014]. The GCM-RCM coupling approach transforms GCM biases through RCM lateral and lower boundaries, which could affect the interior climate of RCMs. Many approaches have been developed to correct GCM biases at the regional scale. *Ehret et al*. [2012] presented a comprehensive overview of state-of-the-art bias correction methods and discussed related assumptions, shortcomings, and implications. *Holland et al*. [2010] and *Done et al*. [2013] developed an approach that corrects only the bias of GCM climatological means on the basis of NCEP reanalysis data and allows the GCM variance to change in the future so that the RCM can develop its own interior solution within the bias-corrected boundary data. *Xu and Yang* [2012] improved this approach

by considering inter-annual variations, in addition to the climatological means. *Bruyère et al*. [2013] compared these two approaches and found that corrections of inter-annual variations achieve only marginal improvements. *White and Toumi* [2013] compared the climatological bias correction and quantile-quantile mapping methods [*Colette et al*., 2012] and showed that the former method is more reliable and accurate. *Xu and Yang* [2015] improved their earlier approach [*Xu and Yang*, 2012] by applying weak spectral nudging in addition to the bias correction; they found that the new approach significantly improves the downscaled climatological mean air temperature, geopotential height, and wind vectors.

This study performs high-spatial-resolution (12 km) WRF simulations over a very large domain (7200 km × 6180 km) to explore changes in mean and extreme precipitation over North America. We use GCM outputs from the CMIP5 archive to project future precipitation for two time periods (mid and late 21st century), under two different scenarios (RCP 4.5 and RCP 8.5 hereafter). We also explore the effects of bias correction on model performance for a historical simulation and future precipitation projections. Section 2 describes the model, the bias correction method, and the evaluation data sets; section 3 presents historical evaluations at seasonal, daily, and sub-daily scales; section 4 discusses changes in precipitation and their uncertainties. Summary and discussion follow in section 5.

2. Methodology

2.1. Global Climate Model

The GCM used in this study is a single model run by the Community Climate System Model version 4 (CCSM4) at a resolution of 0.9° × 1.25° (latitude/longitude) as part of the CMIP5 archive. A historical run and two future runs are named "CCSM run b40.20th.track1.1deg.012," "CCSM run b40.rcp8_5.1deg.007," and "b40.rcp4_5.1deg.006," respectively. This is the only member (of a six-member ensemble for future runs) that saves the outputs every 6 h, providing details at the sub-daily scale and making the model suitable for driving RCMs. CCSM4 is a coupled climate model with components representing the atmosphere, ocean, sea ice, and land surface, as described in detail by *Gent et al*. [2011]. Available output includes historical runs and future runs. The historical runs retain the original external climate forcing but contain observed changes in atmospheric composition (reflecting both anthropogenic and natural sources). The future runs are forced with specified concentrations (greenhouse gas and aerosol) per different scenarios. This study uses projections generated by CCSM4 for two scenarios adopted by the CMIP5—RCP 4.5 and RCP 8.5—which represent a possible range of radiative forcing values in the year 2100 relative to pre-industrial values (+4.5 and +8.5 W m^{-2}, respectively). See *Meinshausen et al*. [2011] and *Peacock* [2012] for more details.

2.2. Bias Correction

This study applies the approach tested by *Bruyère et al*. [2013], which corrects the mean errors in the GCM but retains the GCM's 6 h weather, longer-period climate variability, and climate change [Figure 1 in *Xu and Yang*, 2012; Figure 4 in *Bruyère et al*., 2013]. Thus, it allows the variance, diurnal cycle, seasonal cycle, and phase of inter-annual variations to change freely from the past to future periods. In this study, we correct the atmospheric components of CCSM4 (used as boundary conditions for the downscaling) by using the NCEP–National Center for Atmospheric Research Reanalysis Project (NNRP) data [*Kalnay et al*., 1996] over the period 1950–1979, which we define as the base period. This period is chosen because it has no significant climate trend, and thus no trend needs to be removed before bias correction. The process used is described below.

First, the 6 h NNRP data and CCSM4 outputs are broken down into a climatological mean plus a perturbation term:

$$\mathrm{CCSM} = \overline{\mathrm{CCSM}} + \mathrm{CCSM}'$$

$$\mathrm{NNRP} = \overline{\mathrm{NNRP}} + \mathrm{NNRP}'$$

Accordingly, the CCSM4 model output for the three time periods we model (1994–2004, 2044–2054, and 2084–2094) can be written as follows:

$$\mathrm{CCSM}_c = \overline{\mathrm{CCSM}_c} + \mathrm{CCSM}'_c = \left(\overline{\mathrm{CCSM}_b} - \overline{\mathrm{NNRP}_b}\right) + \overline{\mathrm{NNRP}_b} + \left(\overline{\mathrm{CCSM}_c} - \overline{\mathrm{CCSM}_b}\right) + \mathrm{CCSM}'_c$$

The subscripts b and c represent the base period (1950–1979) and the considered period (1994–2004, 2044–2054, or 2084–2094), respectively. Thus, the bias-corrected CCSM4 data CCSM_c^* in the three considered periods are constructed by removing the CCSM4's climatological bias $\overline{\mathrm{CCSM}_b} - \overline{\mathrm{NNRP}_b}$:

$$\begin{aligned}\mathrm{CCSM}_c^* &= \overline{\mathrm{NNRP}_b} + \left(\overline{\mathrm{CCSM}_c} - \overline{\mathrm{CCSM}_b}\right) + \mathrm{CCSM}_c' \\ &= \left(\overline{\mathrm{NNRP}_b} - \overline{\mathrm{CCSM}_b}\right) + \overline{\mathrm{CCSM}_c} + \mathrm{CCSM}_c' \\ &= \left(\overline{\mathrm{NNRP}_b} - \overline{\mathrm{CCSM}_b}\right) + \mathrm{CCSM}_c\end{aligned}$$

The corrected atmospheric variables include zonal and meridional wind, geopotential height, temperature, and relative humidity every 6 h, for three dimensions. The bias in sea surface temperature (SST) is corrected by using Analysis SST data, which merges Hadley Centre and National Oceanic and Atmospheric Administration optimum interpolation SST data sets [*Hurrell et al*., 2008] over the period 1950–1979. These variables were tested by *Bruyère et al*. [2013] and found to be the most important for GCM bias corrections. In addition, we correct the land/sea mask in the land surface model by replacing "land" with "sea" over the Great Lakes region, as first recommended by *Gao et al*. [2012] in a sensitivity study showing that modification of the land/sea mask could significantly reduce the bias of the 2 m air temperature near the Great Lakes simulated by the Weather Research and Forecasting (WRF) model.

2.3. Regional Climate Model

This study uses the WRF model version 3.3.1 to dynamically downscale CCSM4 in one historical period (1995–2004) and two future periods (2045–2054 and 2085–2094) under RCP 4.5 and RCP 8.5. The WRF model is applied at a horizontal resolution of 12 km, with 600 west-east × 515 south-north grid points and 28 vertical levels over most of North America [Figure 1 in *Wang and Kotamarthi*, 2014] (WK14 hereafter). The physics schemes used in this study include the Grell-Devenyi convective parameterization [*Grell and Devenyi*, 2002], the Yonsei University planetary boundary layer scheme [*Noh et al*., 2003], the Noah land surface model [*Chen and Dudhia*, 2001], the longwave and shortwave radiative schemes of the Rapid Radiation Transfer Model for GCM applications (http://rtweb.aer.com) [*Iacono et al*., 2008], and the Morrison microphysics scheme [*Morrison et al*., 2009]. Weak interior nudging is applied above 850 hPa to wavelengths around 1200 km, with a nudging coefficient of 3×10^{-5} s^{-1}. In both historical and future simulations, a 1 year spin-up period is allowed for the model to reach equilibrium. These physics schemes and model setup were applied and tested by WK14 for WRF driven by NCEP-R2 over the same model domain. Among these physics schemes, the Morrison reduced the wet bias in winter over the Great Plains and North Rockies (Figures 8a and 8c in WK14). Weaker nudging and a longer spin-up time reduced the wet bias in summer over the Great Plains. In addition, combining the weaker nudging with the bias correction improved the RCM performance versus only applying bias correction for the GCM [*Xu and Yang*, 2015].

To assess the impacts of bias correction for the CCSM4 boundary conditions, two sets of dynamical downscaling are carried out: uncorrected CCSM4-driven WRF (No_BC_WRF hereafter) for the historical period and bias-corrected CCSM4-driven WRF (BC_WRF hereafter) for the late 21st century. These two sets of simulations use the same model setup, physics schemes, and interior nudging, and they allow the same spin-up time.

2.4. Evaluation Data Sets

We employ North American Regional Reanalysis (NARR) data [*Mesinger et al*., 2006; *Bukovsky and Karoly*, 2007] from multiple sources (aircraft, satellite, stations, etc.) [Tables 1 and 2 in *Mesinger et al*., 2006] to evaluate model performance at seasonal, daily, and sub-daily scales over North America. In wide use by the climate downscaling community [e.g., *Bowden et al*., 2012; *Otte et al*., 2012; *Liu et al*., 2011; *Loikith et al*., 2013], NARR has shown fairly good consistency with observations, although inaccuracies remain in some regions [*Bukovsky and Karoly*, 2007]. To understand the possible bias of NARR data, we compare NARR data with high-resolution (4 km) monthly precipitation data—Precipitation-Elevation Regressions on Independent Slopes Model (PRISM)—developed by *Daly et al*. [1994, 2008]. The PRISM data are corrected for systematic

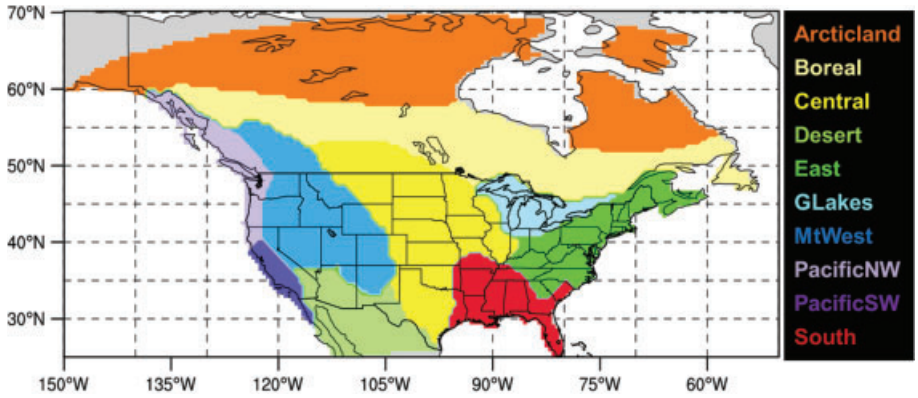

Figure 1. The 10 compound subregions evaluated in this study: Arcticland, Boreal, Central, Desert, East, Great Lakes (GLakes), Mountain West (MtWest), Northwestern Pacific (PacificNW), Southwestern Pacific (PacificSW), and South.

elevation effects on precipitation climatology and are the most accurate, best available data set for evaluating high-resolution model simulations over the Contiguous United States (CONUS).

We employ the geoclimatic subregions developed by *Bukovsky* [2011] for subregional evaluations. We select 10 compound subregions over land (Figure 1), as did *Martynov et al*. [2013]: Arcticland, Boreal, Central, Desert, East, Great Lakes (GLakes), Mountain West (MtWest), Northwestern Pacific (PacificNW), Southwestern Pacific (PacificSW), and South.

3. Evaluation of Historical Simulations

3.1. Climatological Mean

Figure 2 shows seasonal mean precipitation for NARR, No_BC_WRF, BC_WRF, and CCSM4 (uncorrected), as well as differences between model simulations and NARR in the warm (April to September) and cold (October to March) seasons during 1995–2004. In general, both WRF and CCSM4 generate precipitation patterns similar to NARR, with the heaviest precipitation over the eastern domain in the warm season and over the northwestern domain in the cold season. However, as Figure 3a shows, CCSM4 overestimates the precipitation in both seasons over the western domain (e.g., Desert, MtWest, PacificNW, western Canada, and Alaska) and East. In addition, CCSM4 produces a dry bias over South in the cold season. Both No_BC_WRF and BC_WRF reduce the biases over Desert, MtWest, and East. In particular, the unrealistic convective precipitation in the warm season over western CONUS found in the CCSM4 is effectively removed. BC_WRF shows smaller bias than No_BC_WRF over Desert, MtWest, and PacificSW in the warm season and over Desert, MtWest, PacificSW, East, and South in the cold season. However, No_BC_WRF and BC_WRF still show strong wet biases (up to 4 mm) over the Rocky Mountains and Cascades at a very small scale. This is because NARR, with a relatively coarse resolution, might not be able to capture the small-scale precipitation at relatively high elevations. Comparisons between NARR and PRISM over CONUS show that NARR underestimates the precipitation in the cold season by 1–3 mm at many isolated locations over the Rocky Mountains and Cascades. This indicates that the wet bias of WRF simulations over these locations is perhaps not as strong as shown here. In comparison with No_BC_WRF, BC_WRF generates larger wet bias over Canada (e.g., Arcticland) and central CONUS (e.g., Central).

3.2. Heavy Precipitation

We evaluate model performance in heavy precipitation according to percentiles. Figures 4 and 5 show the 75th and 95th percentiles, respectively, of daily precipitation in winter (December, January, February) and summer (June, July, August) over North American. Figures 3b and 3c show the regional average bias over the 10 subregions defined in Figure 1. For the 75th percentile (Figure 4), in winter CCSM4 shows the heaviest precipitation and the largest wet bias over Alaska, Desert, MtWest, and PacificNW. Both No_BC_WRF and BC_WRF effectively reduce the wet bias over these regions. This is also the case for percentiles below the 75th. No_BC_WRF underestimates precipitation over South at and below the 75th percentile, and the dry bias is stronger and wider than in CCSM4 and in BC_WRF. BC_WRF generates larger bias than No_BC_WRF over Canada, Central, GLakes, PacificNW, and PacificSW. In summer, CCSM4 shows the heaviest precipitation

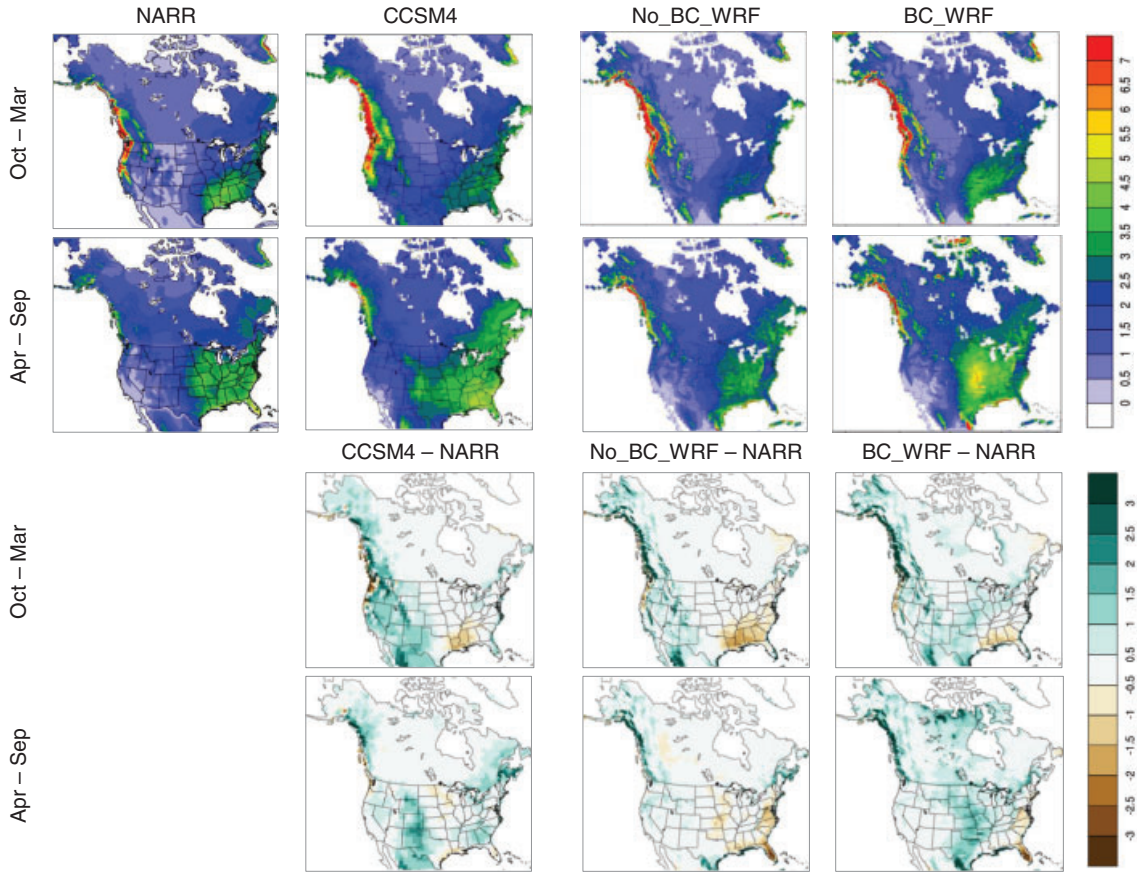

Figure 2. NARR-, CCSM4-, and WRF-simulated 10 year mean precipitation (mm d^{-1}; top two rows), with bias of CCSM4 and WRF versus NARR (mm d^{-1}; bottom two rows), during October–March and April–September.

and the largest wet bias over Desert, MtWest, and South. No_BC_WRF and BC_WRF reduce the bias over MtWest and over most southeastern states except Florida. Although No_BC_WRF underestimates the precipitation over most of the 10 subregions, BC_WRF reduces the dry bias or generates a wet bias versus NARR. This difference exists for precipitation at and below the 75th percentile.

The bias is generally larger for the 95th percentile (Figure 5) than for the 75th percentile. In winter, CCSM4 shows the heaviest precipitation and the largest wet bias over Desert, MtWest, PacificNW, and PacificSW. No_BC_WRF and BC_WRF reduce the wet bias over these regions to some extent, but they both generate more precipitation over Alaska, Central, East, and GLakes. As for the 75th percentile, a strong and wide dry bias is generated by No_BC_WRF over South. BC_WRF reduces the range and the magnitude of this dry bias. However, BC_WRF shows a strong wet bias—the strongest among the three simulations—from Texas to the Great Lakes. In summer, CCSM4 shows a dry bias over the entire central North America and a wet bias over Desert, MtWest, and PacificNW. No_BC_WRF shows a bias pattern similar to that of CCSM4, but it reduces the bias over central Canada, Central, MtWest, and Desert. BC_WRF shows smaller biases than CCSM4 and No_BC_WRF over MtWest and Desert, but it generates much more precipitation over Arcticland, Boreal, Central, GLakes, and South than does NARR.

In summary, model bias clearly varies according to precipitation percentile. In comparison with No_BC_WRF, BC_WRF captures the lower-percentile events more realistically than the extreme events. However, BC_WRF has a tendency toward excessive precipitation during heavy storms. CCSM4 overestimates both the lower-percentile and extreme events over MtWest and Desert in both seasons.

3.3. Precipitation Frequency

To explore the effects of bias correction on WRF model performance further, Figure 6 shows the differences in precipitation frequency for No_BC_WRF and BC_WRF versus NARR. The precipitation frequency is defined

(a) Seasonal mean		A	B	C	D	E	GL	MW	PN	PS	S
Oct – Mar	CCSM4 – NARR	0.20	0.16	0.38	1.17	0.17	0.03	1.42	2.36	0.54	-0.52
	No_BC WRF – NARR	0.13	0.08	0.15	0.78	-0.17	-0.20	0.97	1.93	0.29	-0.63
	BC_WRF – NARR	0.41	0.27	0.60	0.69	-0.02	0.38	0.97	2.45	-0.19	-0.14
Apr – Sep	CCSM4 – NARR	0.50	0.14	0.24	0.58	0.43	0.33	0.70	0.77	0.09	0.20
	No_BC WRF – NARR	0.32	-0.04	-0.01	-0.07	-0.14	0.03	0.44	0.87	0.15	-0.13
	BC_WRF – NARR	1.10	0.38	0.98	0.07	-0.29	0.76	0.39	1.18	0.01	0.26

(b) 75th Percentile		A	B	C	D	E	GL	MW	PN	PS	S
DJF	CCSM4 – NARR	0.55	0.70	0.50	0.90	-0.17	0.32	1.62	2.13	0.91	-0.30
	No_BC WRF – NARR	0.09	0.14	0.06	0.33	-0.23	-0.16	0.78	0.22	-0.44	-0.90
	BC_WRF – NARR	0.31	0.40	0.46	0.34	0.18	0.66	0.85	1.28	-1.06	-0.34
JJA	CCSM4 – NARR	0.89	0.36	1.02	1.32	1.21	1.97	1.52	0.21	0.15	1.01
	No_BC WRF – NARR	-0.25	-0.41	-0.37	-0.68	1.05	0.48	0.42	-0.24	0.19	-0.42
	BC_WRF – NARR	1.15	0.48	1.54	-0.46	1.08	1.97	0.48	0.25	0.18	0.25

(c) 95th Percentile		A	B	C	D	E	GL	MW	PN	PS	S
DJF	CCSM4 – NARR	1.21	1.65	3.01	9.02	1.51	2.01	5.24	7.93	6.32	-1.06
	No_BC WRF – NARR	1.04	1.37	1.94	7.38	1.02	1.52	4.46	6.56	5.69	-1.56
	BC_WRF – NARR	1.64	1.68	3.86	5.96	2.09	3.78	4.51	7.72	2.77	1.46
JJA	CCSM4 – NARR	2.10	1.20	-3.57	0.88	1.05	-0.50	1.50	2.80	0.60	-0.50
	No_BC WRF – NARR	2.07	1.87	0.07	-0.76	5.30	4.95	1.32	2.00	0.91	1.43
	BC_WRF – NARR	5.44	3.42	5.08	-0.26	3.66	7.10	1.01	2.77	0.59	3.25

Figure 3. (a) Seasonal averaged bias of CCSM4- and WRF-simulated precipitation (mm d^{-1}) versus NARR based on monthly data; (b) 75th percentile of CCSM4- and WRF-simulated precipitation (mm d^{-1}) versus NARR based on daily data; (c) 95th percentile of CCSM4- and WRF-simulated precipitation (mm d^{-1}) versus NARR based on daily data. The bars represent the values of bias for a given model and subregion. Wet bias is indicated by blue or green color, while dry bias is indicated by orange or red color. Note the bars are not comparable across tables. The subregions are A, Acticland; B, Boreal; C, Central; D, Desert; E, East; GL, Great Lakes; MW, Mountain West; PN, Northwestern Pacific; PS, Southwestern Pacific; S, South.

as the number of days per year with precipitation greater than 1, 5, or 10 mm, for 10 year daily precipitation simulated by No_BC_WRF and BC_WRF during 1995–2004. Generally, both WRF simulations overestimate the precipitation frequency for all types of precipitation over the western domain (e.g., Rocky Mountains and Alaska). No_BC_WRF underestimates the precipitation frequency over Central, GLakes, East, South, and Boreal. BC_WRF produces more precipitation days over GLakes, East, South, and Boreal and reduces the bias of precipitation frequency generated by No_BC_WRF. This is one of the important improvements made by BC_WRF, which captures the precipitation occurrences better than No_BC_WRF over much of eastern CONUS. However, BC_WRF produces too many days with heavy precipitation (5 and 10 mm) over Central, which is one of the main reasons for the wet bias of precipitation in the warm season over this region (Figures 2, 4, and 5).

We also examine the bias of precipitation intensity simulated by No_BC_WRF and BC_WRF versus NARR (Figure S1, Supporting Information). The intensity is defined as the ratio of total precipitation amount in 10 years to the total days with precipitation greater than 1 mm. Although both WRF simulations overestimate the precipitation intensity over the western domain (from Desert to Alaska), BC_WRF generates more intense precipitation over southern Central, Midwest, and South.

In summary, bias correction improves the model's performance in both precipitation frequency and intensity over South. This results in smaller bias of precipitation amount than for the non-corrected simulation. However, the bias correction induces more frequent, more intense precipitation over Central and thus yields a much greater precipitation amount than NARR and the non-corrected simulation.

3.4. Diurnal Variation of Precipitation

The diurnal cycle of precipitation, in comparison with the sub-synoptic and synoptic cycles, is the dominant mechanism for summer precipitation over most of CONUS, as shown by *Castro et al*. [2007]. By investigating the diurnal variations of precipitation, *Tripathi and Dominguez* [2013] found that their model produced

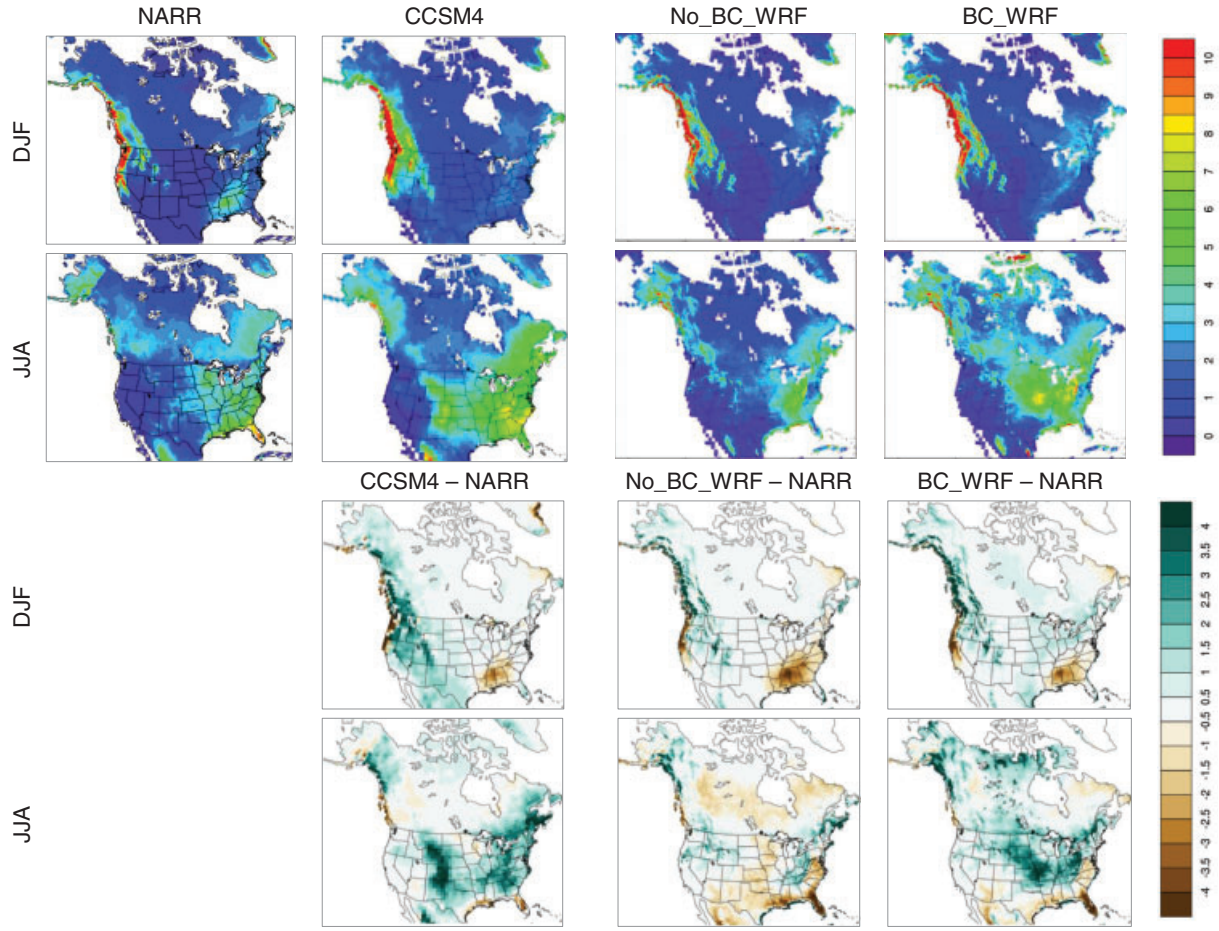

Figure 4. 75th percentile of NARR-, CCSM4-, and WRF-simulated daily precipitation (mm d^{-1}; top two rows), with bias of CCSM4 and WRF versus NARR (mm d^{-1}; bottom two rows) in winter (DJF: December, January, February) and summer (JJA: June, July, August).

slower propagation of the rainfall system and heavier hourly rainfall than observations, thus inducing a wet bias in the climatological mean. To explore the causes for the wet/dry bias shown in this study (Figures 2–5) and to evaluate model performance at the sub-daily scale, Figure 7 compares diurnal variations in precipitation for NARR, No_BC_WRF, BC_WRF, and CCSM4 in May–August of 1995–2004, averaged along 30–40°N. For NARR, the rainfall peak over 100–105°W occurs at around 00–06 UTC, and then the rainfall system moves eastward to 92–100°W at around 06–12 UTC. Later, rainfall reaches a maximum over 85–92°W at around 18–00 UTC. CCSM4 generates a rainfall peak over 85–92°W, but it is ~3 h earlier than the NARR peak. In addition, CCSM4 does not generate the second rainfall peak that NARR shows at around 06–12 UTC over 92–100°W. In contrast, CCSM4 generates heavier rainfall over 103–105°W from 18 UTC to the next 06 UTC, which does not exist in NARR. This is why CCSM4 shows much heavier precipitation than observations (Figure 2) over 100–110°W (near MtWest). No_BC_WRF and BC_WRF do not have such a long rainfall duration over 100–110°W, thus reducing the wet bias over MtWest.

As convective processes are dominant in the diurnal cycle of summer precipitation, the differences between CCSM4 and WRF simulations (Figures 7b–d) indicate that the treatments of precipitation process are different in CCSM4 and WRF. No_BC_WRF captures the rainfall peak around 18–00 UTC near 85–96°W, but it does not capture the second rainfall peak around 06–12 UTC over 92–100°W. This is a leading reason why the precipitation generated by No_BC_WRF over South in the summer is less than the NARR values. BC_WRF generates too much rainfall near 92–96°W, especially from 18 UTC to the next 03 UTC. This produces the strong BC_WRF wet bias for summer precipitation over Central, especially the areas near Missouri and Kansas.

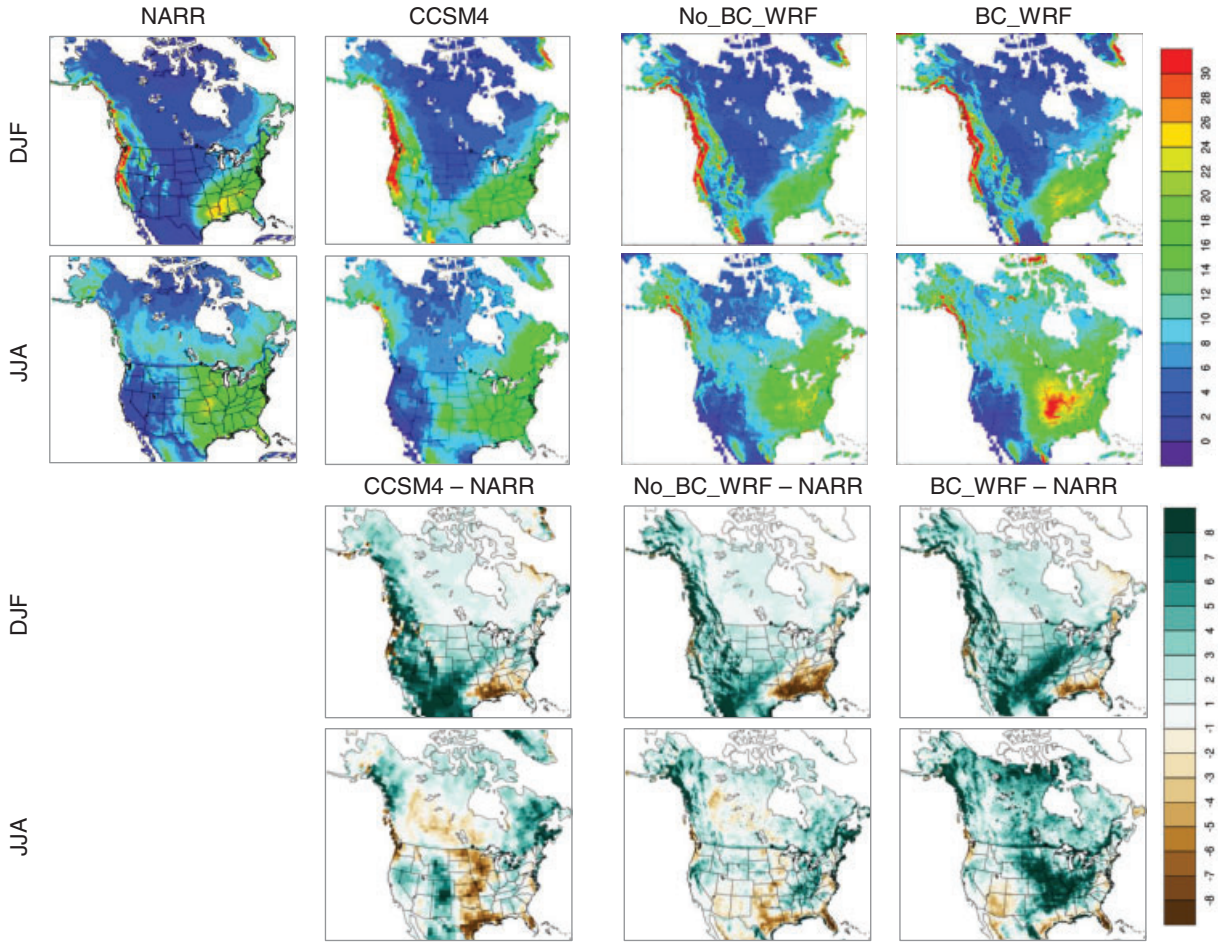

Figure 5. 95th percentile of NARR-, CCSM4-, and WRF-simulated daily precipitation (mm d^{-1}; top two rows), with bias of CCSM4 and WRF versus NARR (mm d^{-1}; bottom two rows) in winter (DJF: December, January, February) and summer (JJA: June, July, August).

4. Projections of Future Precipitation

4.1. Climatological Means

As shown in section 2.2, the bias correction approach applied in this study corrects only the climatological mean of CCSM4 and allows the data ($CCSM_c^*$) to change freely at sub-daily, daily, seasonal, and yearly scales. Therefore, the original CCSM4 and corrected CCSM4 have the same variabilities for those corrected atmospheric variables. The result is mostly similar changes in precipitation from the historical period to the future, as projected by BC_WRF and No_BC_WRF, although the absolute values for future precipitation projected by BC_WRF and No_BC_WRF are different (Figure S2). We present the future changes projected by BC_WRF in this section. The changes projected by No_BC_WRF are similar in geographic patterns and magnitudes, with differences in magnitude less than 10%.

Figures 8 and 9 show the annual and seasonal mean precipitation changes in the mid and late 21st century (2045–2054 minus 1995–2004 and 2085–2094 minus 1995–2004) under RCP 4.5 and 8.5, as projected by BC_WRF and CCSM4. The precipitation change signals in the late 21st century, especially the wet tendency over Canada and Alaska, are generally stronger for both WRF and CCSM4 than those in the mid 21st century under RCP 8.5. The changes are smaller under RCP 4.5 than under RCP 8.5. The annual means of changes in precipitation show decreases over Desert and the south part of Central under both RCPs, as projected by WRF and CCSM4. The dry signal is stronger and the range is wider in WRF than in CCSM4. In addition, precipitation is increased over PacificNW and much of Canada, and the wet signal over northeastern Canada is statistically significant. The precipitation changes due to RCP scenarios over Alaska in the mid 21st century are significant, with a drier projection by RCP 4.5 versus the historical period and a wetter projection by RCP

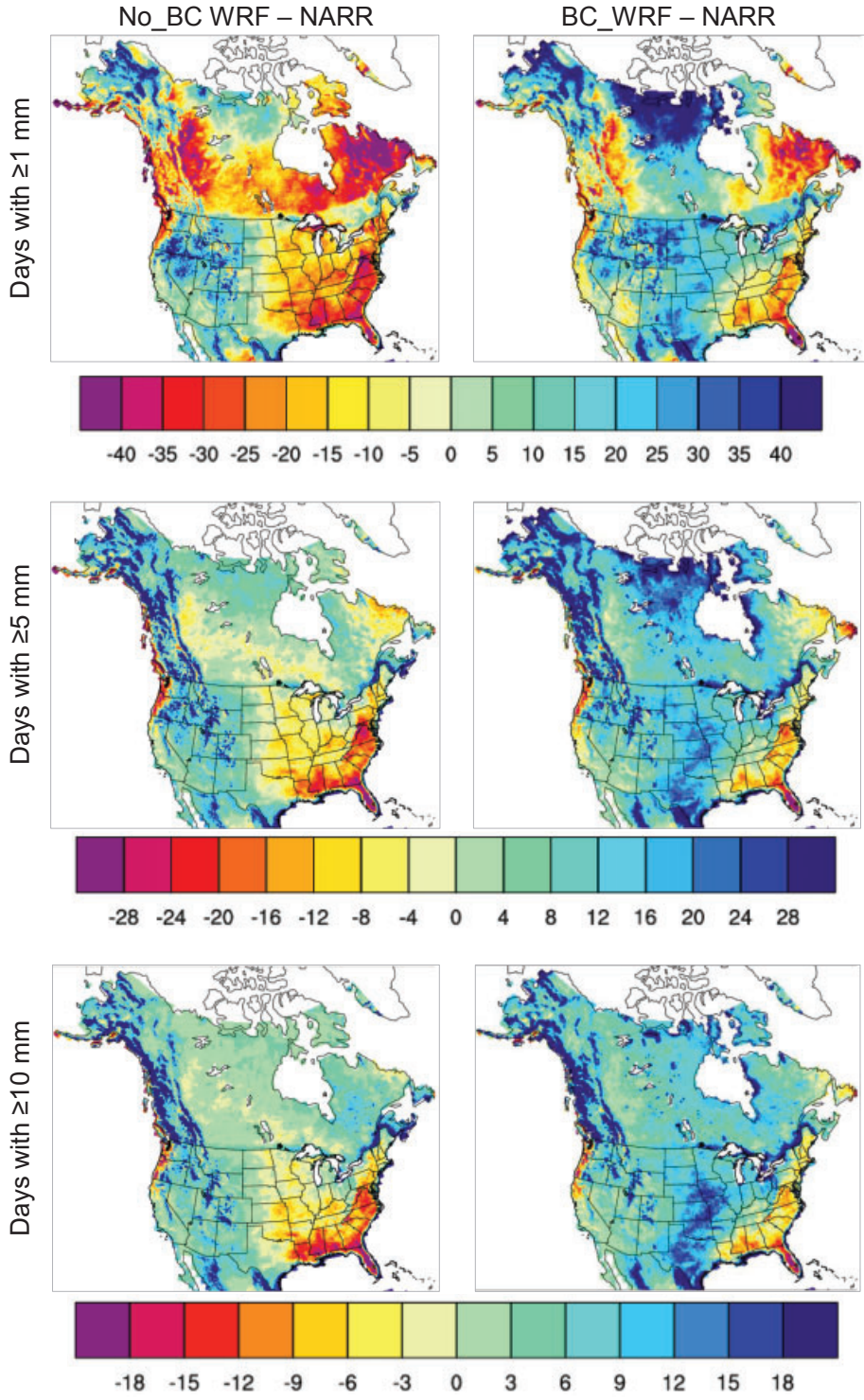

Figure 6. The differences in number of days per year with precipitation amount greater than 1, 5, and 10 mm for No_BC WRF and BC_WRF simulation versus NARR using the 10 year historical simulation (1995 – 2004).

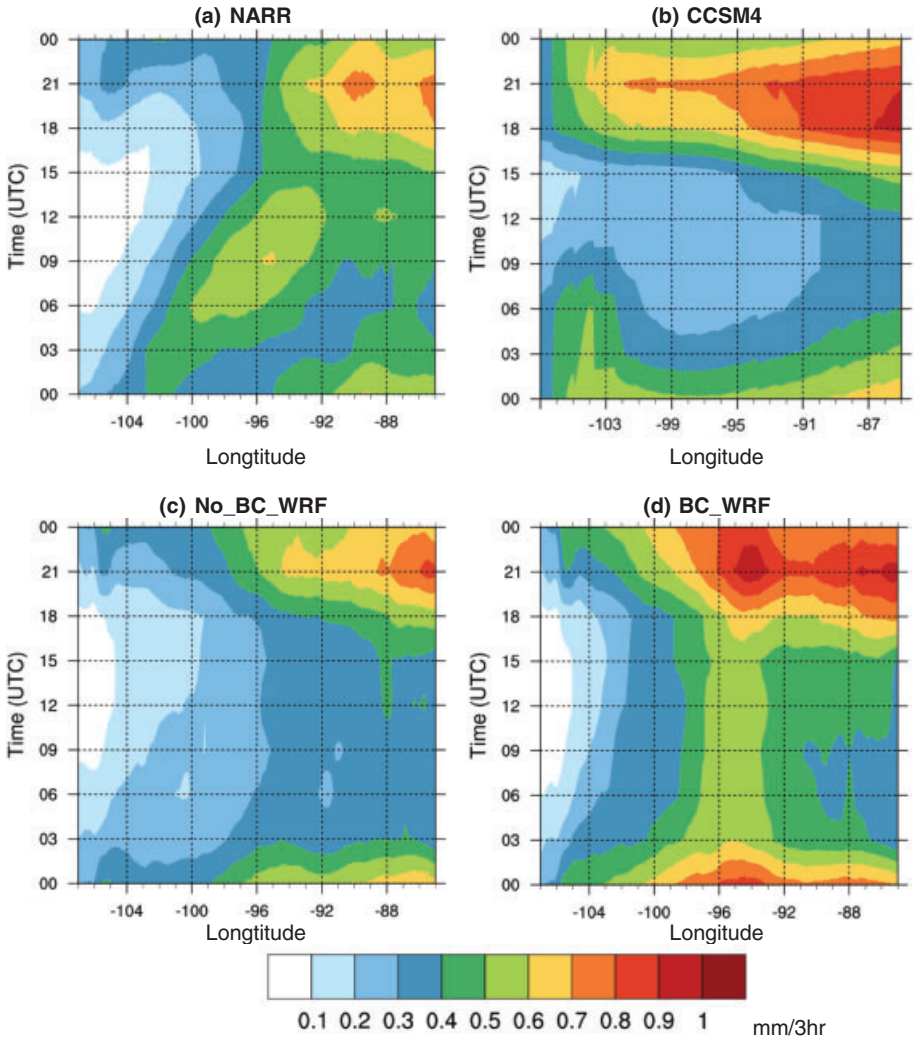

Figure 7. Time-longitude plots (averaged along 30–40°N) of diurnal variation in precipitation simulated by NARR, WRF, and CCSM4 in May–August of 1995–2004.

8.5. Both RCP 4.5 and 8.5 project increased precipitation over Alaska in the late 21st century. WRF also shows increased precipitation over eastern CONUS under RCP 8.5, while the WRF changes under RCP 4.5 and the CCSM4 changes under both RCPs are smaller.

The changes in precipitation show strong dependence on season. A strong decrease in precipitation over Desert and the southern part of Central and MtWest in winter and spring is projected by both WRF and CCSM4. Similar results were found by previous studies using CMIP5 ensemble runs [*Cook and Seager*, 2013] and downscaling simulations [*Gao et al*., 2014]. In contrast, increased precipitation in summer and fall over southwestern CONUS is projected by WRF under RCP 8.5 in 2045–2054, and the increase gains strength in 2085–2094 (Figure 9). On average, the precipitation intensity in summer over this region (mostly North American monsoon region) is projected to increase from 1.8 to 2.3 mm d^{-1} in 2045–2054 and to 2.7 mm d^{-1} in 2085–2094 under RCP 8.5. *Cook and Seager* [2013] also found increased precipitation over Desert and the Southwest in September and October by using 41 CMIP5 ensemble members. *Torres-Alavez et al*. [2014] found increases in precipitation and related moisture flux in both summer and fall over Desert and the Southwest in six CMIP5 model runs. On the other hand, slight increases in wet conditions over the eastern United States are projected in spring by both WRF and CCSM4 and in summer by WRF. CCSM4 and WRF show similar patterns and signs (increase or decrease) for precipitation changes in winter, spring, and fall, but the magnitude is somewhat weaker in CCSM4 projections than in WRF projections. However, the changes

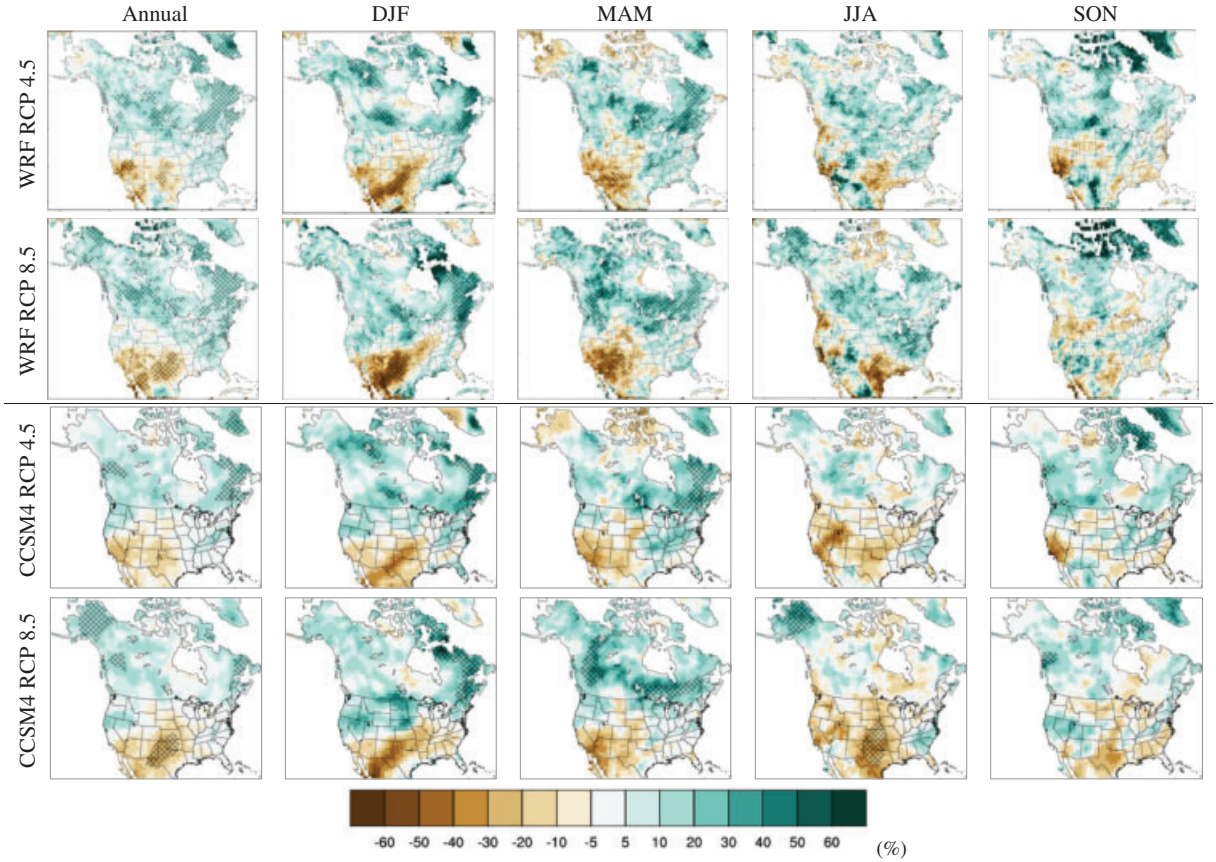

Figure 8. BC_WRF- and CCSM4-projected change (%) in seasonal and annual mean precipitation for 2045–2054 versus 1995–2004 and for RCP 4.5 and RCP 8.5. Cross-hatching indicates statistically significant changes. Seasons: DJF: December, January, February; MAM: March, April, May; JJA: June, July, August; SON: September, October, November.

of precipitation projected by WRF for summer differ from those projected by CCSM4, and the differences under RCP 8.5 are significant.

Because physics representations in RCMs are different from those in GCMs [*Han and Roads*, 2004; *Liang et al*., 2006], transformation from GCM to RCM results in redistribution of the influxes of mass, energy, and momentum in the RCM domain. This is a direct consequence of different representations of key physical processes, especially land-atmosphere-ocean and convection-cloud-radiation interactions [e.g., *Liang et al*., 2004a, 2004b]. *Han and Roads* [2004] compared the performance of an RCM and a GCM and found that the large differences between the RCM and the GCM are mainly due to differences in model physics (such as the cumulus parameterization) rather than differences in grid resolution, especially when the sub-grid processes are important, as during summer. *Liang et al*. [2006], *Pan et al*. [2001, 2004], and *Han and Roads* [2004] compared the changes projected by an RCM and a GCM and found that patterns of precipitation change are significantly different in summer.

In this study, we investigate the differences between WRF and CCSM4 in summer in the past versus the future (2085–2094) under RCP 8.5. Here we simply compare CCSM4 with No_BC_WRF, instead of BC_WRF. In the historical period, CCSM4 (Figure 10a) shows an overestimation (up to 3 mm) in comparison with NARR precipitation over much of North America, except over central and southern Canada. WRF effectively reduces the wet and dry bias over these regions (Figure 10b) because of the possible improvement of cumulus parameterization in WRF. In the future period, the geographic patterns of differences between WRF and CCSM4 are similar to those in the historical period, except for the western United States, Boreal, Midwest, and East (Figure 10c). This indicates that, as stated by *Liang et al*. [2008], some of the bias in CCSM4 is systematically propagated from the historical into the future period. However, in comparison with Figure 10b, Figure 10c shows weaker negative values over the western United States and stronger

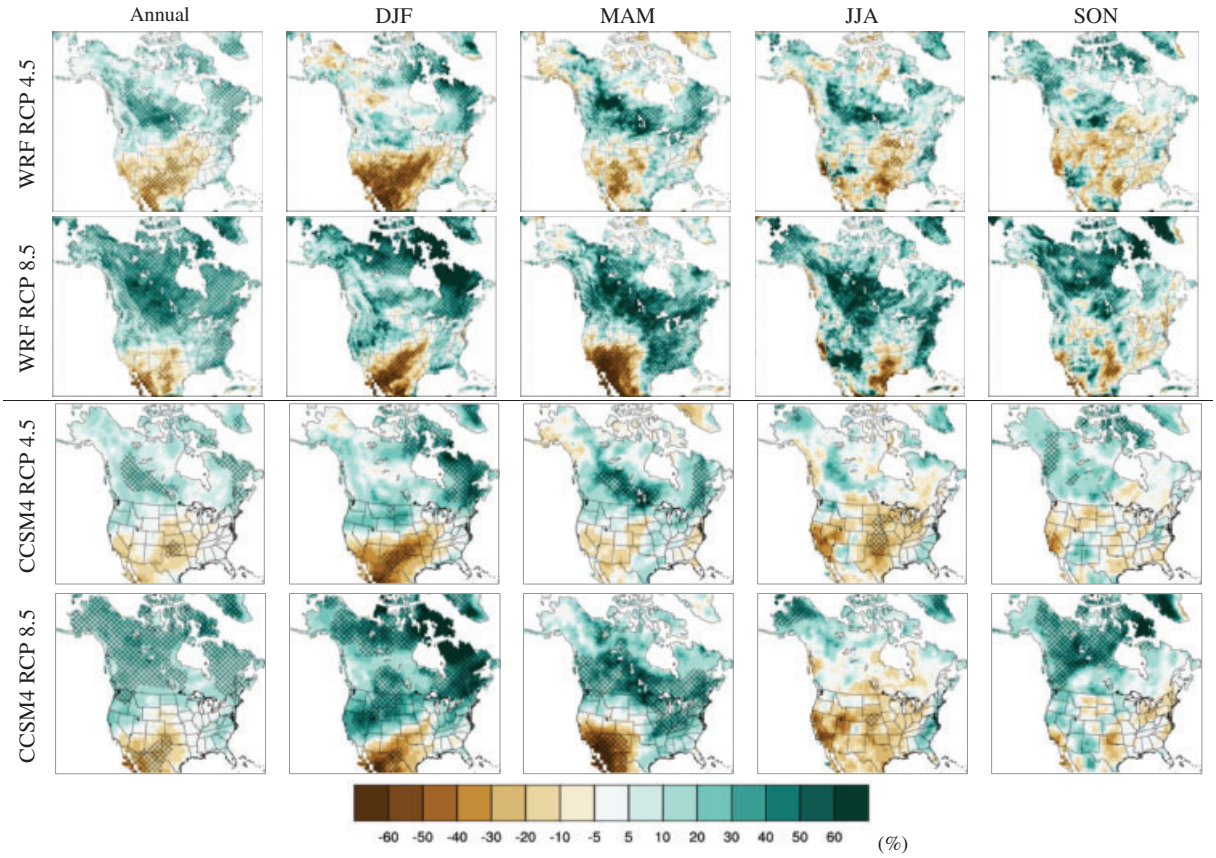

Figure 9. BC_WRF- and CCSM4-projected change (%) in seasonal and annual mean precipitation for 2085–2094 versus 1995–2004 and for RCP 4.5 and RCP 8.5. Cross-hatching indicates statistically significant changes. Seasons: DJF: December, January, February; MAM: March, April, May; JJA: June, July, August; SON: September, October, November.

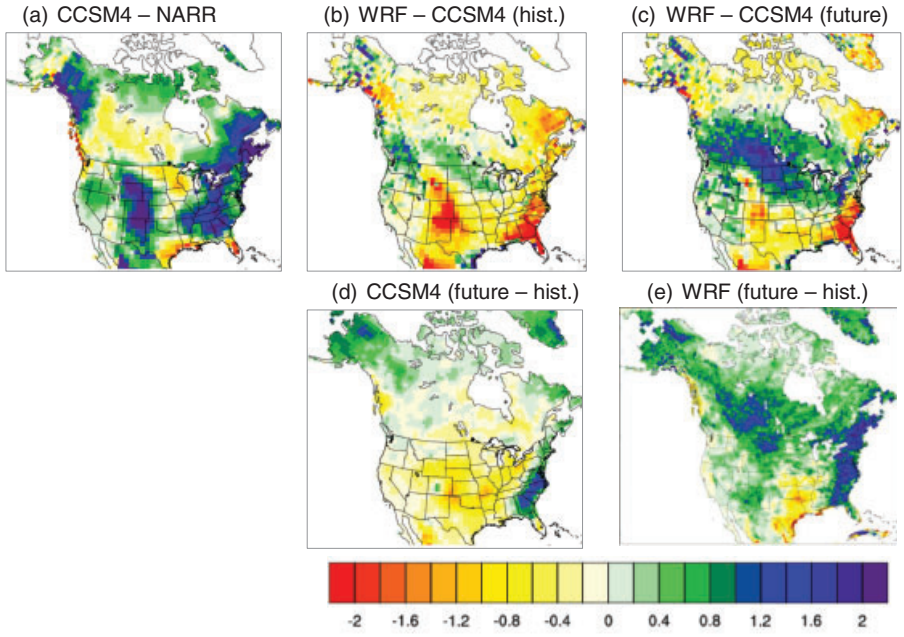

Figure 10. (a) CCSM4 bias in summer (June, July, August) precipitation versus NARR; (b–c) differences between WRF and CCSM4 in historical (1995–2004) and future (2085–2094) periods under RCP 8.5; (d–e) absolute changes in summer (June, July, August) precipitation projected by CCSM4 and WRF (2085–2094 minus 1995–2004) under RCP 8.5.

positive values over Boreal and the Midwest. For example, over central and southern Canada, WRF is higher than CCSM4 by only 0.2 mm in the historical period (Figure 10b), while it is higher than CCSM4 by 1.2 mm in the future (Figure 10c), though CCSM4 projects only a 0.2 mm (or less) decrease of precipitation in the future (Figure 10d). This induces a 0.8 mm increase of precipitation in the future, as simulated by WRF (Figure 10e). The differences between the changes projected by WRF and CCSM4 over southwestern CONUS can be explained similarly. In fact, for the regions where the difference (WRF minus CCSM4) does not change too much (e.g., over southeastern CONUS) from the historical period to the future (Figures 10b and 10c), the precipitation changes projected by CCSM4 and WRF are very similar (Figures 10d and 10e).

In summary, it is possible that the precipitation values simulated/projected by RCMs and GCMs differ because of different physical processes for generating precipitation. If these differences between RCMs and GCMs do not change from the historical to the future period, then the RCM and GCM project similar changes in the future. This study, however, shows that the differences between precipitation simulated/projected by RCMs and GCMs can change over time, and thus the climate changes projected by RCMs and GCMs can be different, especially in summer. Additional tests show that the differences in future changes of precipitation between BC_WRF and CCSM4 have the same explanation.

In comparison with CCSM4, WRF projects a cooler and wetter future in the summer over much of North America under RCP 8.5 in the late 21st century, consistent with the findings of *Liang et al*. [2006]. We acknowledge, however, that possible uncertainties in the climate change signals projected by WRF need to be investigated by running more downscaling simulations driven by additional GCMs.

4.2. Precipitation Percentiles and Heavy Precipitation

Figure 11 shows the percentage changes in precipitation at percentiles from the 55th to the 99th along 35–40°N in 2085–2094 under RCP 4.5 and RCP 8.5. We first determine that the point of the 55th percentile from an ascending rank of 10 year daily data is the 2007th data point. Thus, the time series from the 2007th to the 3650th includes all the daily precipitation values >55th percentile. Each data point between the 2007th and the 3650th has a percentile value. For the very low precipitation values, even a small absolute change in rainfall can cause a large shift in percentage change. For moderate to high precipitation events, the percentage change is fairly consistent as a function of rainfall intensity for each RCP. Generally, the projected changes in precipitation percentiles are similar between WRF and CCSM4 in the mid 21st century in all four seasons (Figure S3), while the changes in summer are different at the end of the 21st century. In the mid 21st century (2045–2054), both CCSM4 and WRF project decreased precipitation over the Southwest in winter, spring, and summer; strong increases over the Southwest in fall; and increases over the Southeast in spring, summer, and fall. In the late 21st century (2085–2094), the patterns of precipitation change are similar to those in the mid 21st century, except that in summer the WRF projects increased precipitation over southwestern CONUS under RCP 8.5.

Figure 12 shows changes in precipitation at percentiles from the 55th to the 99th along 40–45°N in 2085–2094 under RCP 4.5 and RCP 8.5. Although the CCSM4 and WRF precipitation projections in different seasons are somewhat different at lower percentiles, both models project increased precipitation at and above the 95th percentile, as well as increased precipitation over the Northwest in winter and spring in both the mid and late 21st century. For example, in wintertime of the mid 21st century (Figure S4), both WRF and CCSM4 project increases in precipitation at and above the 95th percentile over 95–125°W along 40–45°N. In summertime, both models project increases in extreme precipitation over 80–120°W, although the CCMS4 signal is weaker than the WRF signal. In the late 21st century, extreme precipitation tends to increase in all four seasons over much of CONUS along 40–45°N, as projected by both WRF and CCSM4 under RCP 8.5.

Figure 13 shows the changes in days per year (considering inter-annual variability) with specified precipitation amounts (1–10, 10–20, and 20–40 mm) for the 10 year historical period (1995–2004) versus two 10 year periods in the future (2045–2054 and 2085–2094). As the precipitation threshold is increased, fewer days in the historical and future periods experience these conditions, as expected. Although relatively light precipitation (1–10 mm) shows larger changes in days per year than does heavier precipitation (10–20 and 20–40 mm), the changes in days with light precipitation show larger variabilities due to inter-annual variations. For the 10 year average changes, all subregions show increases in days with all types of precipitation except for Desert, which shows few days or a decrease in days. Among the 10 subregions, PacificNW

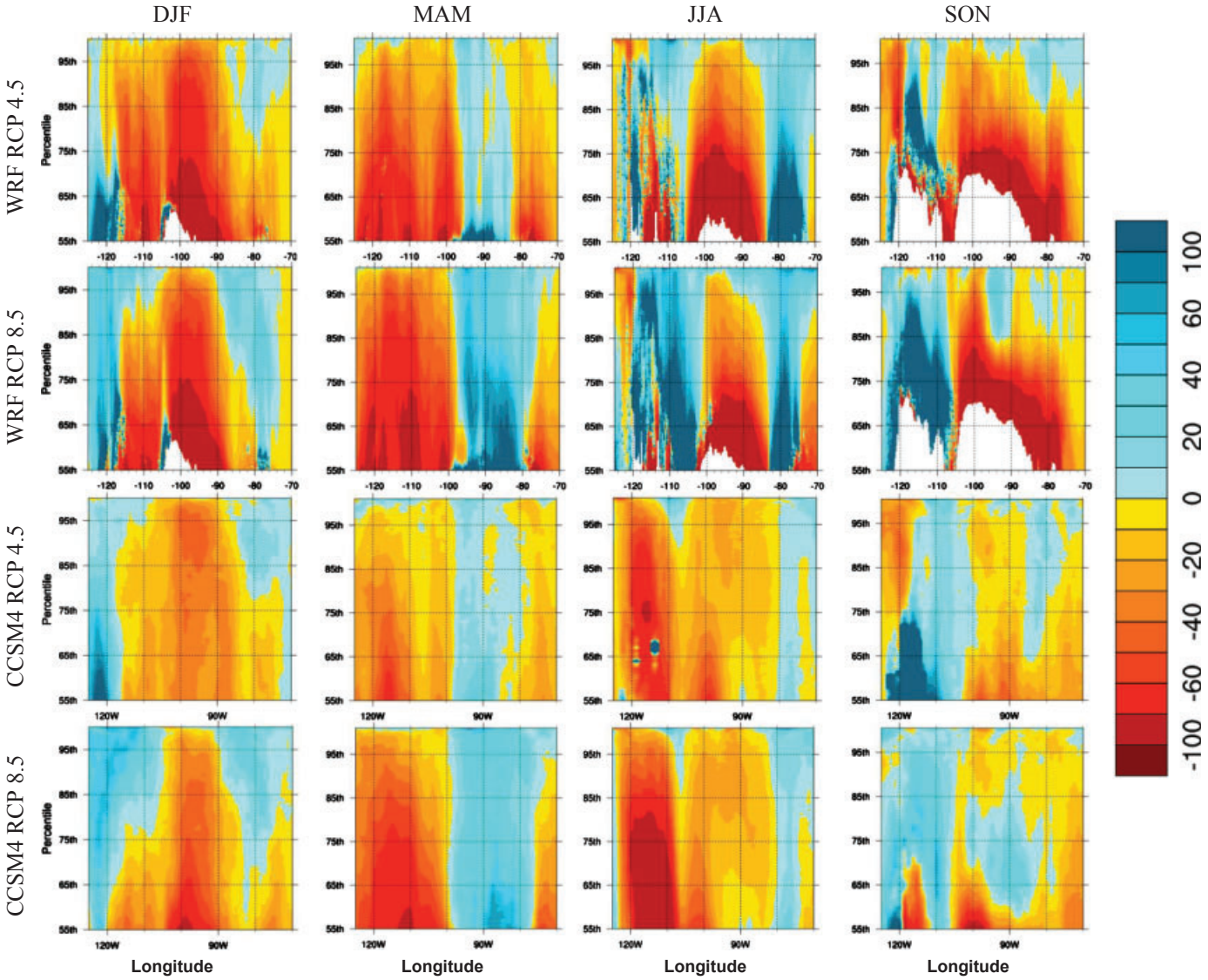

Figure 11. WRF- and CCSM4-projected change (%) in percentiles (55th to 99th) of precipitation for 1995–2004 versus 2085–2094 under RCP 4.5 and RCP 8.5, averaged along 35–40°N.

shows the largest change in days with 10–20 and 20–40 mm in the mid and late 21st century under both RCPs, occurring mostly in fall and winter (Figure 12). East shows the second largest change in days of all types of precipitation, occurring mostly in spring and summer (Figure 12). Considering the inter-annual variability of both the historical and future periods, we find a wide spread for changes in days with specified precipitation, especially in 2045–2054 under both RCPs. In 2085–2094, the spread of inter-annual variability is narrower, and days with 10–20 mm of precipitation show clear increases over much of North America.

Figure 14 shows the changes in frequency (occurrences per year) of 2 day duration 5 year return events and 2 day duration 10 year return events for the historical period (1995–2004) versus future periods (2045–2054 and 2085–2094), obtained with the method of *Janssen et al*. [2014]. Duration refers to the number of days over which precipitation is accumulated, and return is an average of the number of years between events. Thus, the frequency of an event in a given time series depends only on the return time and the length of the time series. In the historical period, we have 365 events of 2 day duration and 5 year return and ~183 events of 2 day duration and 10 year return. To count the number of occurrences of these events in the future period, we first determine thresholds for a given duration and return from the historical simulations. We then

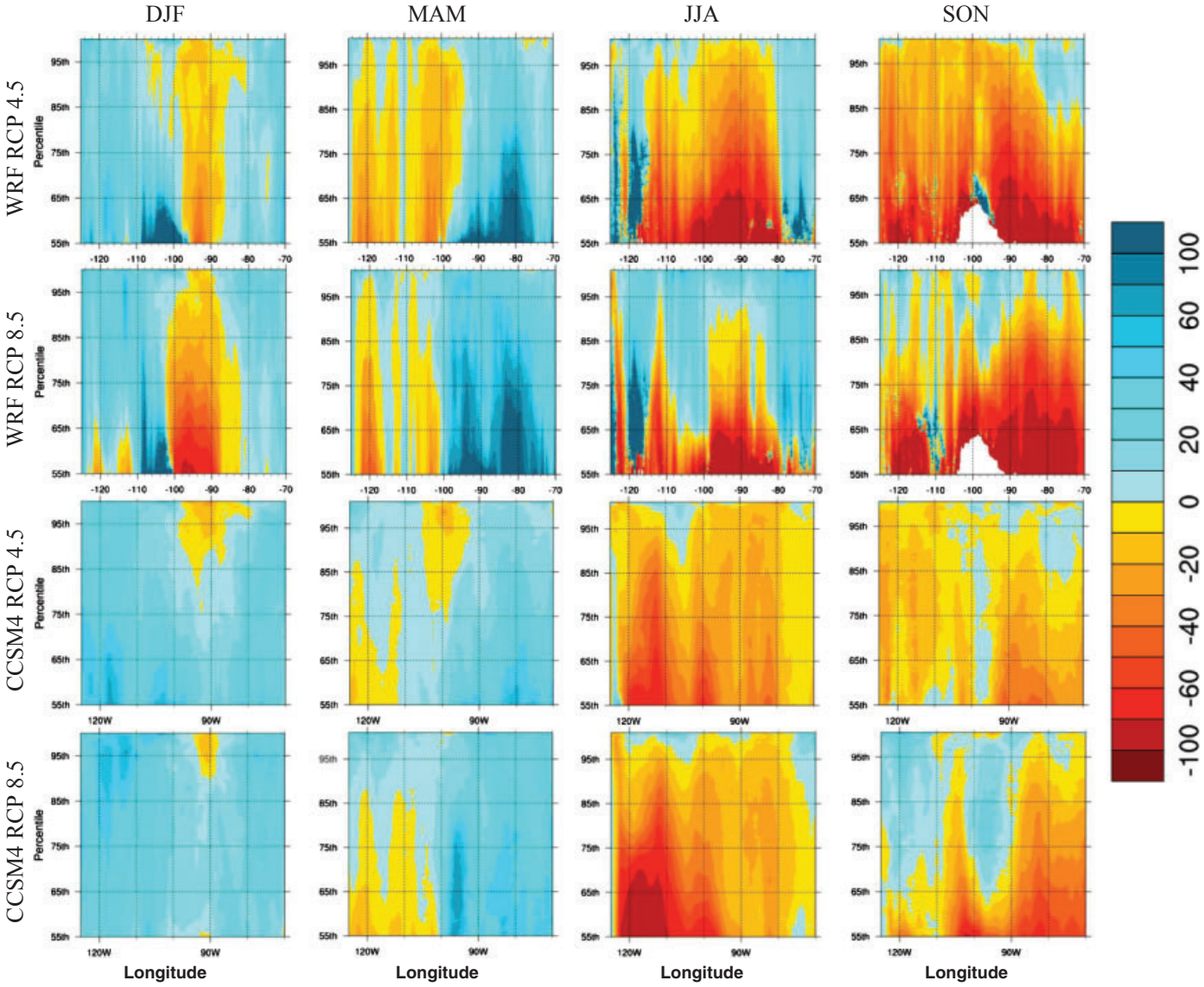

Figure 12. WRF- and CCSM4-projected change (%) in percentiles (55th to 99th) of precipitation for 1995–2004 versus 2085–2094 under RCP 4.5 and RCP 8.5, averaged along 40–45°N.

apply those thresholds to the projections to identify the events exceeding the thresholds and compare the number of these events in future periods with the number in the historical period.

In 2085–2094, we find increases of 2 day events with 5 and 10 year returns over much of North America except Desert and PacificSW, which show decreases of frequency under both RCPs. The largest increases of frequency are over Arcticland and Boreal. In contrast, PacificNW and East (Figure 13) show the largest increases of frequency of heavy precipitation. This indicates that long-duration events tend to increase more than short-duration and intense events over Arcticland and Boreal. The 2 day duration events over South show a slight decrease under RCP 4.5, but Figure 13 shows a significant increase for precipitation. This indicates that the long-duration events tend to decrease, while the short-duration and intense events tend to increase in the future over South. Over Desert, all types of events (long and short duration) are projected to be less frequent. We find similar changes in frequency of 2 day events with 5 and 10 year returns over most of the 10 subregions in the mid 21st century, but the frequencies of these events over Central and South are projected to decrease under RCP 4.5.

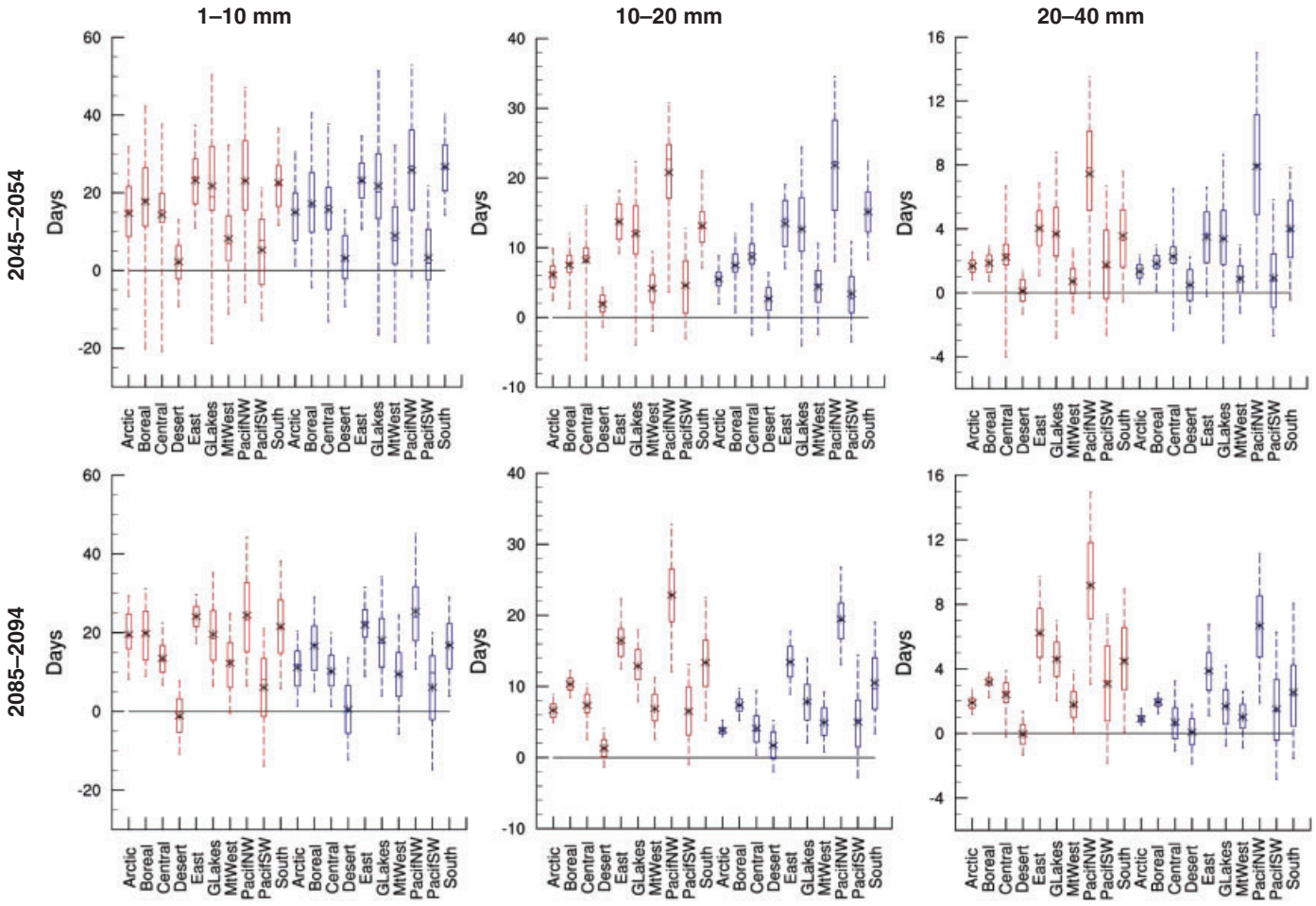

Figure 13. WRF-projected changes in days of different types of precipitation for 1995–2004 versus 2045–2054 (top row) and for 1995–2004 versus 2085–2094 (bottom row) under RCP 8.5 (red boxes) and RCP 4.5 (blue boxes), considering inter-annual variabilities. Boxes indicate the 25th and 75th quantiles, with the horizontal line indicating the median and the whiskers showing the extreme range of inter-annaual variability. The stars indicate the 10 year average change between the histroical and future periods.

5. Summary and Discussion

We use WRF simulations driven by the uncorrected and bias-corrected CCSM4 for two different future warming scenarios, with 10 year historical data (1995–2004) and two 10 year future time slices (2045–2054 and 2085–2094), to investigate (1) the impacts of bias correction on model performance in the historical period; (2) the value added by WRF beyond CCSM4; and (3) projected changes in mean and extreme precipitation in the future. BC_WRF reduces the bias of mean precipitation generated by No_BC_WRF in the cold season and shows smaller bias than No_WRF_BC for precipitation at and below the 75th percentile in winter over South. BC_WRF also improves the model performance in precipitation frequency, especially over South and East. However, BC_WRF overestimates mean and extreme precipitation in the warm season over Central and the precipitation frequency and intensity over central North America. A possible reason for the wet bias over Central (mostly over Kansas and Missouri) in summer is the convective parameterization. WK14 conducted a 4 km run with convective parameterization turned off and showed reduced wet bias over the northern Great Plains by ~30% versus the control simulation for the Grell-Devenyi convective parameterization. Another possible reason is that spectral nudging, even with a weak strength, could overestimate precipitation (Figure 8c in WK14).

Both BC_WRF and No_BC_WRF add important value beyond the CCSM4 by reducing the wet bias over the western domain and showing much more detail than CCSM4 in spatial and diurnal variation of precipitation over much of CONUS. This result indicates that the WRF simulation at 12 km resolves the observed fine-scale features more realistically than does the driving GCM, which enhances the credibility of future

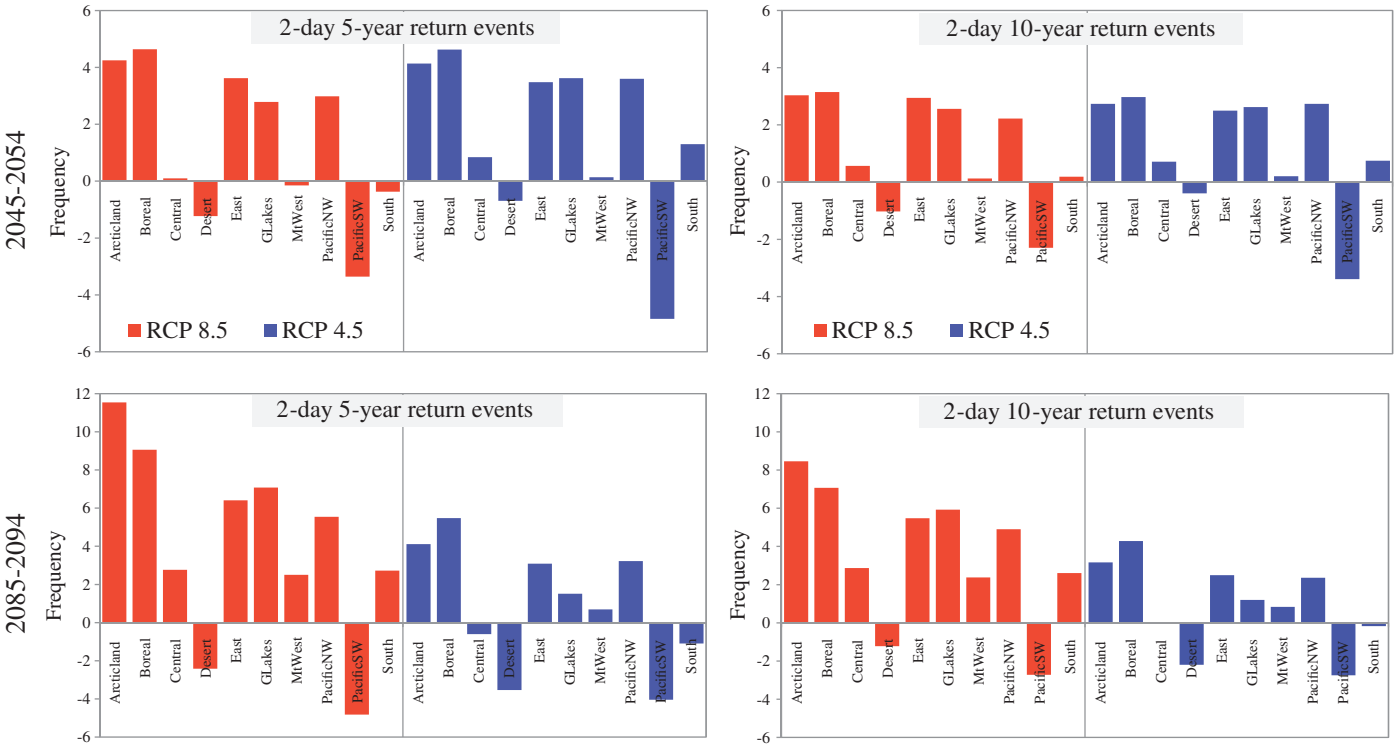

Figure 14. WRF-projected changes in frequency (number of occurrences per year) of 2 day duration 5 year return and 2 day duration 10 year return events for 1995–2004 versus 2045–2054 (top row) and for 1995–2004 versus 2085–2094 (bottom row) under RCP 8.5 (red bars) and RCP 4.5 (blue bars).

climate change projections for regional-scale applications. We acknowledge, however, the possibility of uncertainties in future projections, because only one RCM-GCM pair is applied in this study.

Analysis of the results from WRF simulation at 12 km indicates that precipitation over Desert decreases in winter and spring under both RCPs. Central and eastern CONUS show an increase of precipitation in spring. Canada is found to be wetter in the future under both RCPs for most of the year. At the lower percentiles of precipitation, differences in the estimated changes occur, but extreme precipitation increases over northeastern and southeastern CONUS in most seasons, for both WRF and CCSM4. In addition, the days with heavy precipitation increase over much of North America. This change is larger under RCP 8.5 than under RCP 4.5 for extreme precipitation. The WRF and CCSM4 projections agree on precipitation changes in winter, spring, and fall but show clear differences in precipitation changes in summer. The increase in precipitation is associated with increased specific humidity [*Willett et al*., 2007], water vapor [*Santer et al*., 2007], and surface temperature warming. *Peacock* [2012] found that the percent change of higher percentiles of precipitation change is ~3%/K over North America. *d'Orgeville et al*. [2014] found that average rainfall intensity is expected to increase by 7%/K, while heavy rainfall is expected to increase by 7%–10%/K over the Great Lakes Basin.

While our simulation and previous simulations are not completely comparable because of different GCMs and/or different physics and model setups for RCMs, previous studies gave some similar findings. For example, *Xu and Yang* [2015] applied a similar bias correction approach for a 60 km WRF driven by the Community Atmosphere Model (CAM) and found that, while the bias correction with weaker spectral nudging improves air temperature, geopotential height, and wind, it does not always reduce the bias of precipitation, especially over the southern Great Plains. *Bukovsky and Karoly* [2011] and *Gao et al*. [2014] found that, in comparison with initial and boundary conditions provided by CCSM3 or CCSM4, the WRF at 30 or 25 km improved the realism of the diurnal cycle, the spatial distribution over complex terrain, and the magnitude of heavy 6 h events. For future precipitation change projected by RCMs driven by CCSM3, our review of outputs of NARCCAP (http://www.narccap.ucar.edu/results/index.html#climate-change) indicates that most RCMs driven by CCSM3 show decreases in precipitation over Desert and MtWest in

winter and spring, with increases over Canada. Interestingly, as in this study, the changes in summer projected by RCMs driven by CCSM3 versus CCSM3 itself are mostly opposite in sign.

To further understand of the performance of CCSM4, we review previous studies comparing CCSM4 with other CMIP5 models. *Sheffield et al*. [2013] analyzed North American precipitation in CMIP5 experiments. As documented in their Table 3, CCSM4 shows moderate bias versus observed precipitation in both summer and winter. The regional average biases over North America and CONUS for CCSM4 are mostly smaller than 15%, except that the CCSM4 overestimates the precipitation over MtWest and Desert in winter and underestimates the precipitation over Desert in summer by 40%–50%. For extreme precipitation, *Janssen et al*. [2014] compared 19 models to observations for rainfall events with 2 day duration and 5, 10, and 20 year returns. The two historical ensemble members of CCSM4 show much smaller spread than other CMIP5 models. The correlation coefficients between CCSM4 and observations over CONUS for these extreme events are mostly above 0.5.

Acknowledgments
This work is supported under a military interdepartmental purchase request from the Strategic Environmental Research and Development Program, RC-2242, through U.S. Department of Energy (DOE) contract DE-AC02-06CH11357. The PRISM data are available at http://www.prism.oregonstate.edu/. The NARR data (in NetCDF format) are provided by the NOAA-ESRL Physical Sciences Division, Boulder, Colorado, at http://www.esrl.noaa.gov/psd/. The CCSM4 data are downloaded from https://www.earthsystemgrid.org/home.htm. Computational resources are provided by the DOE-supported Argonne Leadership Computing Facility and the National Energy Research Scientific Computing Center. All the model outputs generated in this study will be available online. We are in the process of setting up access to the data archive.

References

Blanc, E., K. Strzepek, A. Schlosser, H. Jacoby, A. Gueneau, C. Fant, S. Rausch, and J. Reilly (2014), Modeling U.S. water resources under climate change, *Earth's Future*, *2*, 197–224, doi:10.1002/2013EF000214.

Bowden, J. H., T. L. Otte, C. G. Nolte, and M. J. Otte (2012), Examining interior grid nudging techniques using two-way nesting in the WRF model for regional climate modeling, *J. Clim.*, *25*, 2805–2823.

Bowles, D. C., C. D. Butler, and S. Friel (2014), Climate change and health in Earth's future, *Earth's Future*, *2*, 60–67, doi:10.1002/2013EF000177.

Bruyère, C. L., J. M. Done, G. J. Holland, and S. Fredrick (2013), Bias corrections of global models for regional climate simulations of high-impact weather, *Clim. Dyn.*, *43*, 1847–1856, doi:10.1007/s00382-013-2011-6.

Bukovsky, M. S. (2011), *Masks for the Bukovsky Regionalization of North America*. Regional Integrated Sciences Collective, Institute for Mathematics Applied to Geosciences, National Center for Atmospheric Research, Boulder, Colo. [Available at http://www.narccap.ucar.edu/contrib/bukovsky/.] Accessed 19 June 2014.

Bukovsky, M. S., and D. J. Karoly (2007), A brief evaluation of precipitation from the North American Regional Reanalysis, *J. Hydrometeorol.*, *8*, 837–846.

Bukovsky, M. S., and D. J. Karoly (2011), A regional modeling study of climate change impacts on warm-season precipitation in the Central United States, *J. Clim.*, *24*, 1985–2002, doi:10.1175/2010JCLI3447.1.

Castro, C. L., R. A. Pielke Sr., and J. O. Adegoke (2007), Investigation of the summer climate of the contiguous U.S. and Mexico using the regional atmospheric modeling system (RAMS). Part I: Model climatology (1950–2002), *J. Clim.*, *20*, 3866–3887.

Chen, F., and J. Dudhia (2001), Coupling an advanced land surface–hydrology model with the Penn State–NCAR MM5 modeling system. Part I: Model implementation and sensitivity, *Mon. Weather Rev.*, *129*, 569–585.

Christensen, J. H., T. R. Carter, M. Rummukainen, and G. Amanatidis. (2007), Evaluating the performance and utility of regional climate models: The PRUDENCE project, *Clim. Change*, *81*, 1–6.

Christensen, J. H., E. Kjellström, F. Giorgi, G. Lenderink, and M. Rummukainen (2010), Assigning relative weights to regional climate models: Exploring the concept, *Clim. Res.*, *44*, 179–194, doi:10.3354/cr00916.

Colette, A., R. Vautard, and M. Vrac (2012), Regional climate downscaling with prior statistical correction of the global climate forcing, *Geophys. Res. Lett.*, *39*, L13707, doi:10.1029/2012GL052258.

Cook, B. I., and R. Seager (2013), The response of the North American Monsoon to increased greenhouse gas forcing, *J. Geophys. Res.*, *118*, 1690–1699, doi:10.1002/JGRD.50111.

Daly, C., R. P. Neilson, and D. L. Phillips (1994), A statistical-topographic model for mapping climatological precipitation over mountainous terrain, *J. Appl. Meteorol.*, *33*, 140–158.

Daly, C., M. Halbleib, J. I. Smith, W. P. Gibson, M. K. Doggett, G. H. Taylor, J. Curtis, and P. P. Pasteris (2008), Physiographically sensitive mapping of climatological temperature and precipitation across the conterminous United States, *Int. J. Climatol.*, *28*, 2031–2064.

Di Luca, A., R. de Elia, and R. Laprise (2012), Potential for added value in precipitation simulated by high-resolution nested regional climate models and observations, *Clim. Dyn.*, *38*, 1229–1247, doi:10.1007/s00382-011-1068-3.

Diffenbaugh, N. S., M. Scherer, and R. J. Trapp (2013), Robust increases in severe thunderstorm environments in response to greenhouse forcing, *Proc. Natl. Acad. Sci. U.S.A.*, *110*(41), 16,361–16,366.

Done, J. M., G. J. Holland, C. L. Bruyère, L. R. Leung, and A. Suzuki-Parker (2013), Modeling high-impact weather and climate: Lessons from a tropical cyclone perspective, *Clim. Change*, *129*, 381–395, doi:10.1007/s10584-013-0954-6.

d'Orgeville, M., W. R. Peltier, A. R. Erler, and J. Gula (2014), Climate change impacts on Great Lakes Basin precipitation extremes, *J. Geophys. Res. Atmos.*, *119*, 10,799–10,812, doi:10.1002/2014JD021855.

Ehret, U., E. Zehe, V. Wulfmeyer, K. Warrach-Sagi, and J. Liebert (2012), Should we apply bias correction to global and regional climate model data?, *Hydrol. Earth Syst. Sci. Discuss.*, *9*, 5355–5387, doi:10.5194/hessd-9-5355-2012.

Ezer, T., and L. P. Atkinson (2014), Accelerated flooding along the U.S. East Coast: On the impact of sea-level rise, tides, storms, the Gulf Stream, and the North Atlantic Oscillations, *Earth's Future*, *2*, 362–382, doi:10.1002/2014EF000252.

Gao, Y., J. S. Fu, J. B. Drake, Y. Liu, and J.-F. Lamarque (2012), Projected changes of extreme weather events in the eastern United States based on a high resolution climate modeling system, *Environ. Res. Lett.*, *7*(4), 044025, doi:10.1088/1748-9326/7/4/044025.

Gao, Y., L. R. Leung, J. Lu, Y. Liu, M. Huang, and Y. Qian (2014), Robust spring drying in the southwestern U.S. and seasonal migration of wet/dry patterns in a warmer climate, *Geophys. Res. Lett.*, *41*, 1745–1751, doi:10.1002/2014GL059562.

Gensini, V. A., and T. L. Mote (2015), Downscaled estimates of late 21st century severe weather from CCSM3, *Clim. Change*, *129*, 307–321, doi:10.1007/s10584-014-1320-z.

Gent, P. R., et al. (2011), The community climate system model version 4, *J. Clim.*, *24*, 4973–4991.

Giorgi, F., and L. O. Mearns (1991), Approaches to the simulation of regional climate change: A review, *Rev. Geophys.*, *29*(2), 191–216, doi:10.1029/90RG02636.

Giorgi, F., C. Jones, and G. R. Asrar (2009), Addressing climate information needs at the regional level: The CORDEX framework, *WMO Bull.*, *58*(3), 175–183.
Giorgi, F., E.-S. Im, E. Coppola, N. S. Diffenbaugh, X. J. Gao, L. Mariotti, and Y. Shi (2011), Higher hydroclimatic intensity with global warming, *J. Clim.*, *24*, 5309–5324, doi:10.1175/2011JCLI3979.1.
Grell, G. A., and D. Devenyi (2002), A generalized approach to parameterizing convection combining ensemble and data assimilation techniques, *Geophys. Res. Lett.*, *29*(14), 1693, doi:10.1029/2002GL015311.
Han, J., and J. O. Roads (2004), U.S. climate sensitivity simulated with the NCEP regional spectral model, *Clim. Change*, *62*, 115–154.
Hawkins, E., and R. Sutton (2009), The potential to narrow uncertainty in regional climate predictions, *Bull. Am. Meteorol. Soc.*, *90*, 1095–1107, doi:10.1175/2009BAMS2607.1.
Hawkins, E., and R. Sutton (2011), The potential to narrow uncertainty in projections of regional precipitation change, *Clim. Dyn.*, *37*(1–2), 407–418.
Hayhoe, K., et al. (2004), Emissions pathways, climate change, and impacts on California, *Proc. Natl. Acad. Sci. U.S.A.*, *101*(34), 12,422–12,427, doi:10.1073/pnas.0404500101.
Hewitson, B. C., and R. G. Crane (1992), Large-scale atmospheric controls on local precipitation in tropical Mexico, *Geophys. Res. Lett.*, *19*, 1835–1838, doi:10.1029/92GL01423.
Holland, G. J., J. M. Done, C. L. Bruyère, C. Cooper, and A. Suzuki (2010), Model investigations of the effects of climate variability and change on future Gulf of Mexico Tropical Cyclone Activity, paper OTC 20690 presented at the Offshore Technology Conference, Houston, Tex., 3–6 May.
Hurrell, J. W., J. J. Hack, D. Shea, J. M. Caron, and J. Rosinski (2008), A new sea surface temperature and sea ice boundary dataset for the community atmosphere model, *J. Clim.*, *21*, 5145–5153, doi:10.1175/2008JCLI2292.1.
Iacono, M. J., J. S. Delamere, E. J. Mlawer, M. W. Shephard, S. A. Clough, and W. D. Collins (2008), Radiative forcing by long-lived greenhouse gases: Calculations with the AER radiative transfer models, *J. Geophys. Res.*, *113*, D13103, doi:10.1029/2008JD009944.
Janssen, E., D. J. Wuebbles, K. E. Kunkel, S. C. Olsen, and A. Goodman (2014), Observational- and model-based trends and projections of extreme precipitation over the contiguous United States, *Earth's Future*, *2*, *99*–113, doi:10.1002/2013EF000185.
Kalnay, E., et al. (1996), The NCEP/NCAR 40-year reanalysis project, *Bull. Am. Meteorol. Soc.*, *77*, 437–471, doi:10.1175/1520-0477(1996)077<0437:TNYRP>2.0.CO;2.
Kumar, S., D. M. Lawrence, P. A. Dirmeyer, and J. Sheffield (2014), Less reliable water availability in the 21st century climate projections, *Earth's Future*, *2*, 152–160, doi:10.1002/2013EF000159.
Kyle, P., C. Müller, K. Calvin, and A. Thomson (2014), Meeting the radiative forcing targets of the representative concentration pathways in a world with agricultural climate impacts, *Earth's Future*, *2*, 83–98, doi:10.1002/2013EF000199.
Lau, N.-C., and M. J. Nath (2014), Model simulation and projection of European heat waves in present-day and future climates, *J. Clim.*, *27*, 3713–3730, doi:10.1175/JCLI-D-13-00284.1.
Lauer, A., C. Zhang, O. Elison-Timm, Y. Wang, and K. Hamilton (2013), Downscaling of climate change in the Hawaii region using CMIP5 results: On the choice of the forcing fields, *J. Clim.*, *26*, 10,006–10,030, doi:10.1175/JCLI-D-13-00126.1.
Liang, X.-Z., L. Li, A. Dai, and K. E. Kunkel (2004a), Regional climate model simulation of summer precipitation diurnal cycle over the United States, *Geophys. Res. Lett.*, *31*, L24208, doi:10.1029/2004GL021054.
Liang, X.-Z., L. Li, K. E. Kunkel, M. Ting, and J. X. L. Wang (2004b), Regional climate model simulation of U.S. precipitation during 1982–2002, Part 1: Annual cycle, *J. Clim.*, *17*, 3510–3528.
Liang, X.-Z., J. Pan, J. Zhu, K. E. Kunkel, J. X. L. Wang, and A. Dai (2006), Regional climate model downscaling of the U.S. summer climate and future change, *J. Geophys. Res.*, *111*, D10108, doi:10.1029/2005JD006685.
Liang, X.-Z., K. E. Kunkel, G. A. Meehl, R. G. Jones, and J. X. L. Wang (2008), Regional climate models downscaling analysis of general circulation models present climate biases propagation into future change projections, *Geophys. Res. Lett.*, *35*, L08709, doi:10.1029/2007GL032849.
Liu, C., K. Ikeda, G. Thompson, R. Rasmussen, and J. Dudhia (2011), High-resolution simulations of wintertime precipitation in the Colorado headwaters region: Sensitivity to physics parameterizations, *Mon. Weather Rev.*, *139*, 3533–3553, doi:10.1175/MWR-D-11-00009.1.
Loikith, P. C., B. R. Lintner, J. Kim, H. Lee, J. D. Neelin, and D. E. Waliser (2013), Classifying reanalysis surface temperature probability density functions (PDFs) over North America with cluster analysis, *Geophys. Res. Lett.*, *40*, *3710*–3714, doi:10.1002/GRL.50688.
Loikith, P. C., D. Waliser, H. Lee, J. D. Neelin, B. R. Lintner, S. McGinnis, L. O. Mearns, and J. Kim (2015), Evaluation of large-scale meteorological patterns associated with temperature extremes in the NARCCAP regional climate model simulations, *Clim. Dyn.*, doi:10.1007/s00382-015-2537-x.
Martynov, A., R. Laprise, L. Sushama, K. Winger, L. Šeparović, and B. Dugas (2013), Reanalysis-driven climate simulation over CORDEX North America domain using the Canadian Regional Climate Model, version 5: Model performance evaluation, *Clim. Dyn.*, *41*, 2973–3005, doi:10.1007/s00382-013-1778-9.
Mearns, L. O., et al. (2009), A regional climate change assessment program for North America, *EOS*, *90*, 311–312.
Mearns, L. O., et al. (2012), The North American Regional Climate Change Assessment Program: Overview of phase I results, *Bull. Am. Meteorol. Soc.*, *93*, 1337–1362.
Mearns, L. O., et al. (2013), Climate change projections of the North American Regional Climate Change Assessment Program (NARCCAP), *Clim. Change*, *120*(4), 965–975.
Meehl, G. A., F. Zwiers, J. Evans, T. Knutson, L. Mearns, and P. Whetton (2000), Trends in extreme weather and climate events: Issues related to modelling extremes in projections of future climate change, *Bull. Am. Meteorol. Soc.*, *81*, 427–436.
Meinshausen, E., et al. (2011), The RCP greenhouse gas concentrations and their extensions from 1765 to 2300, *Clim. Change*, *109*, 213–241, doi:10.1007/s10584-011-0156-z.
Mesinger, F., et al. (2006), North American Regional Reanalysis, *Bull. Am. Meteorol. Soc.*, *87*, 343–360.
Morrison, H., G. Thompson, and V. Tatarskii (2009), Impact of cloud microphysics on the development of trailing stratiform precipitation in a simulated squall line: Comparison of one- and two-moment schemes, *Mon. Weather Rev.*, *137*, 991–1007, doi:10.1175/2008MWR2556.1.
Noh, Y., W. G. Cheon, S. Y. Hong, and S. Raasch (2003), Improvement of the K-profile model for the planetary boundary layer based on large eddy simulation data, *Bound. Layer Meteorol.*, *107*, 401–427.
Oh, S.-G., J.-H. Park, S.-H. Lee, and M.-S. Suh (2014), Assessment of the RegCM4 over East Asia and future precipitation change adapted to the RCP scenarios, *J. Geophys. Res. Atmos.*, *119*, 2913–2927, doi:10.1002/2013JD020693.

Otte, T. L., C. G. Nolte, M. J. Otte, and J. H. Bowden (2012), Does nudging squelch the extremes in regional climate modeling? *J. Clim.*, *25*, 7046–7066.
Pan, Z., J. H. Christensen, R. W. Arritt, W. J. Gutowski Jr., E. S. Takle, and F. Otieno (2001), Evaluation of uncertainties in regional climate change simulations, *J. Geophys. Res.*, *106*, 17,735–17,751, doi:10.1029/2001JD900193.
Pan, Z., R. W. Arritt, E. S. Takle, W. J. Gutowski Jr., C. J. Anderson, and M. Segal (2004), Altered hydrologic feedback in a warming climate introduces a "warming hole,", *Geophys. Res. Lett.*, *31*, L17109, doi:10.1029/2004GL020528.
Peacock, S. (2012), Projected twenty-first-century changes in temperature, precipitation, and snow cover over North America in CCSM4, *J. Clim.*, *25*, 4405–4429, doi:10.1175/JCLI-D-11-00214.1.
Pryor, S. C., G. Nikulin, and C. Jones (2012), Influence of spatial resolution on regional climate model derived wind climates, *J. Geophys. Res.*, *117*, D03117, doi:10.1029/2011JD016822.
Santer, B. D., et al. (2007), Identification of human-induced changes in atmospheric moisture content, *Proc. Natl. Acad. Sci. U.S.A.*, *104*, 15,248–15,253, doi:10.1073/pnas.0702872104.
Sheffield, J., et al. (2013), North American climate in CMIP5 experiments. Part I: Evaluation of historical simulations of continental and regional climatology, *J. Clim.*, *26*, 9209–9245, doi:10.1175/JCLI-D-12-00592.1.
Sillmann, J., V. V. Kharin, X. Zhang, F. W. Zwiers, and D. Bronaugh (2013a), Climate extremes indices in the CMIP5 multimodel ensemble: Part 1. Model evaluation in the present climate, *J. Geophys. Res. Atmos.*, *118*, 1716–1733, doi:10.1002/JGRD.50203.
Sillmann, J., V. V. Kharin, F. W. Zwiers, X. Zhang, and D. Bronaugh (2013b), Climate extremes indices in the CMIP5 multimodel ensemble: Part 2. Future climate projections, *J. Geophys. Res. Atmos.*, *118*, 2473–2493, doi:10.1002/JGRD.50188.
Sobolowski, S., and T. Pavelsky (2012), Evaluation of present and future North American regional climate change assessment program (NARCCAP) regional climate simulations over the southeast United States, *J. Geophys. Res.*, *117*, D01101, doi:10.1029/2011JD016430.
Stoner, A. M. K., K. Hayhoe, X. Yang, and D. J. Wuebbles (2012), An asynchronous regional regression model for statistical downscaling of daily climate variables, *Int. J. Climatol.*, *33*, 2473–2494, doi:10.1002/joc.3603.
Taylor, K. E., R. J. Stouffer, and G. A. Meehl (2012), An overview of CMIP5 and the experiment design, *Bull. Am. Meteorol. Soc.*, *93*, 485–498, doi:10.1175/BAMS-D-11-00094.1.
Torres-Alavez, A., T. Cavazos, and C. Turrent (2014), Land–sea thermal contrast and intensity of the North American Monsoon under climate change conditions, *J. Clim.*, *27*, 4566–4580, doi:10.1175/JCLI-D-13-00557.1.
Trail, M., A. P. Tsimpidi, P. Liu, K. Tsigaridis, Y. Hu, A. Nenes, and A. G. Russell (2013), Downscaling a global climate model to simulate climate change over the US and the implication on regional and urban air quality, *Geosci. Model Dev.*, *6*, 1429–1445.
Tripathi, O. P., and F. Dominguez (2013), Effects of spatial resolution in the simulation of daily and subdaily precipitation in the southwestern US, *J. Geophys. Res. Atmos.*, *118*, 7591–7605, doi:10.1002/JGRD.50590.
van der Linden, P., and J. F. B. Mitchell (2009), *ENSEMBLES: Climate Change and Its Impacts: Summary of Research and Results from the ENSEMBLES Project*. Met Office, Exeter, U. K., 160 pp.
Vautard, R., et al. (2013), The simulation of European heat waves from an ensemble of regional climate models within the EURO-CORDEX project, *Clim. Dyn.*, *41*(9–10), 2555–2575.
Wang, J., and V. R. Kotamarthi (2014), Downscaling with a nested regional climate model in near-surface fields over the contiguous United States, *J. Geophys. Res. Atmos.*, *119*, 8778–8797, doi:10.1002/2014JD021696.
Wang, J., F. N. U. Swati, M. L. Stein, and V. R. Kotamarthi (2015), Model performance in spatiotemporal patterns of precipitation: New methods for identifying value added by a regional climate model, *J. Geophys. Res. Atmos.*, *120*, 1239–1259, doi:10.1002/2014JD022434.
White, R. H., and R. Toumi (2013), The limitations of bias correcting regional climate model inputs, *Geophys. Res. Lett.*, *40*, 2907–2912, doi:10.1002/GRL.50612.
Willett, K. M., N. P. Gillett, P. D. Jones, and P. W. Thorne (2007), Attribution of observed surface humidity changes to human influence, *Nat. Lett.*, *449*, 710–712, doi:10.1038/nature06207.
Wuebbles, D., et al. (2014), CMIP5 climate model analyses: Climate extremes in the United States, *Bull. Am. Meteorol. Soc.*, *95*, 571–583, doi:10.1175/BAMS-D-12-00172.1.
Xu, C.-Y. (1999), From GCMs to river flow: A review of downscaling methods and hydrologic modelling approaches, *Prog. Phys. Geogr.*, *23*(2), 229–249.
Xu, Z., and Z.-L. Yang (2012), An improved dynamical downscaling method with GCM bias corrections and its validation with 30 years of climate simulations, *J. Clim.*, *25*, 6271–6286.
Xu, Z., and Z.-L. Yang (2015), A new dynamical downscaling approach with GCM bias corrections and spectral nudging, *J. Geophys. Res. Atmos.*, *120*, 3063–3084, doi:10.1002/2014JD022958.
Zhao, Z., S.-H. Chen, M. J. Kleeman, and A. Mahmud (2011), The impact of climate change on air quality related meteorological conditions in California—Part II: Present versus future time simulation analysis, *J. Clim.*, *24*, 3362–3376, doi:10.1175/2011JCLI3850.1.